A Journal of the Gesellschaft Deutscher Chemiker

Angewandte Chemie

50 YEARS International Edition

GDCh

www.angewandte.org

2011—50/12

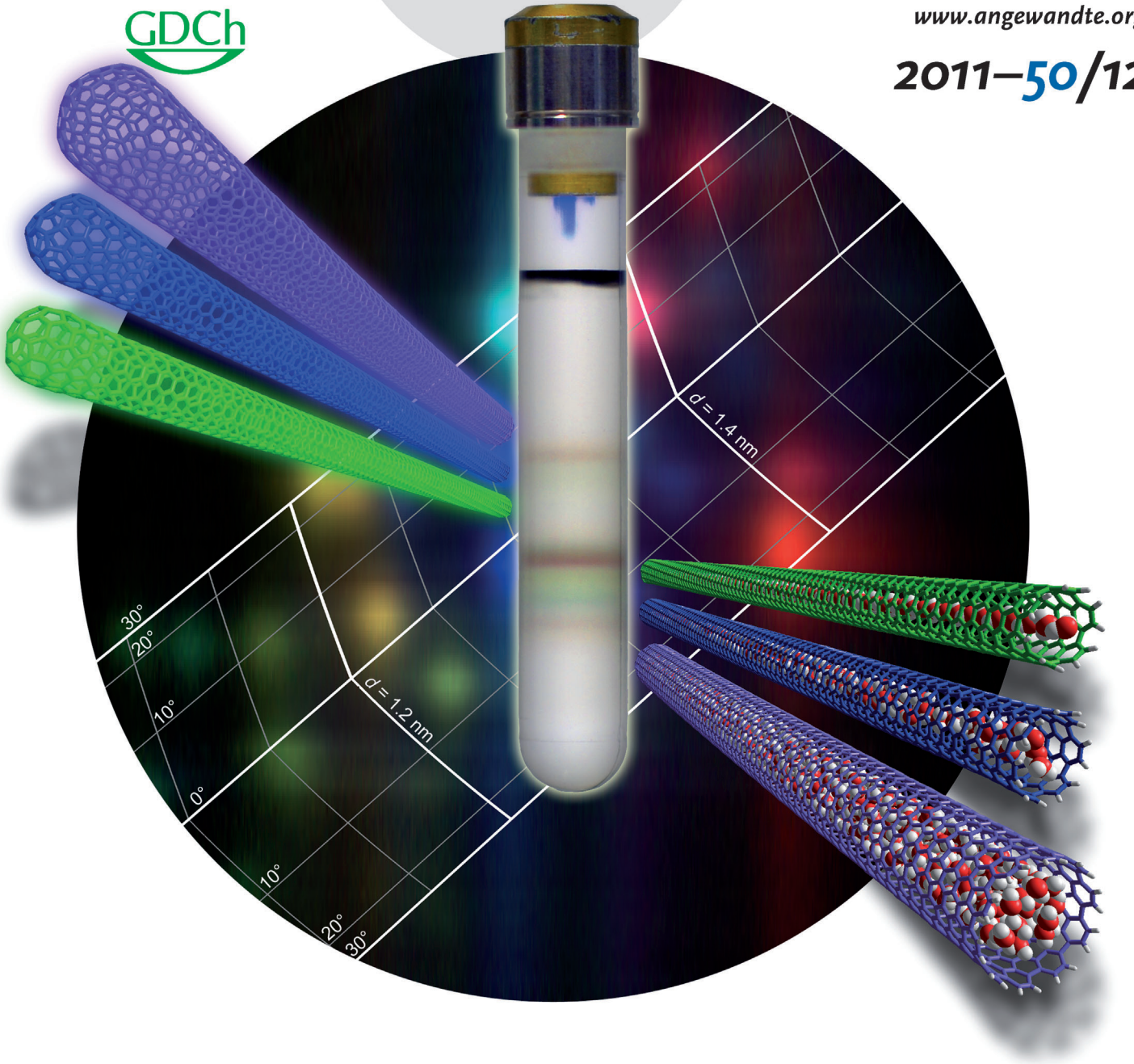

Density-gradient ultracentrifugation ...

... can be used to separate empty (end-capped) and water-filled (open) carbon nanotubes, which coexist in aqueous solutions. As S. Cambré and W. Wenseleers report in their Communication on page 2764 ff., each nanotube chirality can be observed at two different densities, which correspond to empty and water-filled tubes. The separated empty and filled tubes can be further diameter-sorted in one centrifugation run.

WILEY-VCH

Reprint

A Journal of the Gesellschaft Deutscher Chemiker

Angewandte International Edition Chemie

Carbon Nanotubes

Separation and Diameter-Sorting of Empty (End-Capped) and Water-Filled (Open) Carbon Nanotubes by Density Gradient Ultracentrifugation

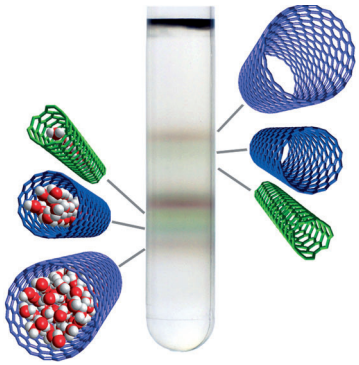

Sorting by spinning: Empty (end-capped) and water-filled (open) carbon nanotubes, which coexist in aqueous solutions, can be separated by density gradient ultracentrifugation (see picture), and the empty tubes allow enhanced diameter sorting. The isolated empty nanotubes possess narrower electronic and vibrational transitions and enhanced quantum efficiences compared to the water-filled nanotubes.

S. Cambré,
W. Wenseleers* _____ **2764 – 2768**

Keywords: carbon nanotubes · chirality · luminescence · surfactants · ultracentrifugation

2011 – 50/12

WILEY-VCH

Carbon Nanotubes

DOI: 10.1002/anie.201007324

Separation and Diameter-Sorting of Empty (End-Capped) and Water-Filled (Open) Carbon Nanotubes by Density Gradient Ultracentrifugation**

*Sofie Cambré and Wim Wenseleers**

Ever since the discovery of single-wall carbon nanotubes (SWCNTs),[1] their unique and remarkably diverse electronic and optical properties, which depend critically on their exact diameter and chiral structure,[2] have proven to be both a blessing and a curse, as synthetic methods invariably produce mixtures of structures, while applications demand more uniform properties. The sorting of SWCNTs by buoyant density through solubilization as individually isolated tubes using bile salt surfactants,[3] followed by ultracentrifugation to equilibrium in a density gradient (DGU), is definitely the most promising technique for separating SWCNTs that have different diameters and chiral structures.[4] However, the diameter-sorting is still not well understood, and the isolation of few or even individual SWCNT species has been limited to SWCNTs with relatively small diameters. In the present work, we have obtained an unprecedented insight into the sorting mechanism by showing that each individual SWCNT chirality actually does not concentrate at one, but rather at two different densities, which correspond to empty and water-filled nanotubes (Figure 1): the intact (end-capped, and therefore empty) SWCNTs, which are present mainly in carefully solubilized samples,[5] can be separated from water-filled SWCNTs by DGU. Remarkably, these empty tubes possess far superior properties than the water-filled tubes used in previous nanotube research, and the overall reversed trend of buoyant density with increasing diameter enhances sorting of large-diameter tubes.

In recent years, important progress has been made toward the preparation of monodisperse SWCNT samples, at least for small-diameter tubes, both by more selective synthesis and by post-synthesis purification methods.[4e,f] The sorting of SWCNTs by DGU was pioneered by Arnold et al.,[4a,6] and has been further developed and emerged as the most widely used and most versatile technique for sorting different SWCNT species by length, diameter, electronic type, and handedness.[4,7] In DGU,[8] particles sediment in a solution of spatially varying density under a high centrifugal acceleration (ca. 10^5 times the standard gravitational acceleration g), until they reach their equilibrium position where their buoyant density matches that of the solution. Counterintuitively,[9] Arnold et al. (and many other DGU studies reported since[4]) found that tubes with larger diameters float at layers that have higher density. A hydrodynamic model, which empirically incorporates a diameter dependence of the surfactant monolayer packing density, has been used to

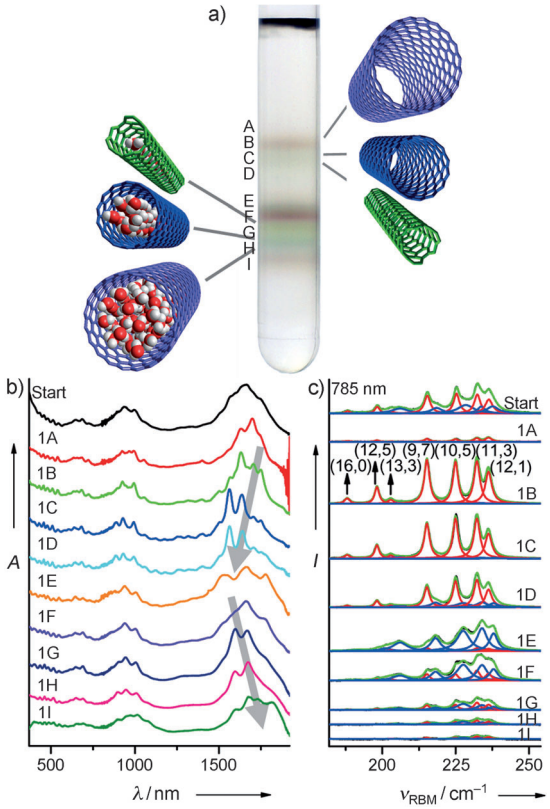

Figure 1. Sorting of empty and water-filled Arc SWCNTs (2% w/v SC). a) Centrifuge tube containing Arc SWCNTs sorted by a 24 h DGU run at 122 000 g in 2% w/v SC solution. Bundles were removed beforehand by medium-speed centrifugation without gradient. b) Absorption spectra of the original solution and of the sorted fractions 1A–1I. Spectra are background-subtracted, normalized, and offset for clarity. c) Resonance Raman spectra (black) of the different fractions excited at 785 nm. Fits (green) are superpositions of the known RBM peaks of empty (red) and filled (blue) tubes. Spectra obtained by excitation at other wavelengths are given in the Supporting Information.

[*] Dr. S. Cambré, Prof. W. Wenseleers
Physics Department, University of Antwerp
Universiteitsplein 1, 2610 Antwerp (Belgium)
Fax: (+32) 3-265-2470
E-mail: wim.wenseleers@ua.ac.be

[**] Financial support from the Fund for Scientific Research Flanders, Belgium (FWO-Vlaanderen; project nos. G.0129.07 and G.0400.11) is gratefully acknowledged. We thank A. Herman, L. Moens, and S. Dewilde for use of the ultracentrifuge.

Supporting information (including experimental details) for this article is available on the WWW under http://dx.doi.org/10.1002/anie.201007324.

describe this reversed order.[10] Theoretical analysis later showed that this model was not sufficient to explain the observed sorting, and prompted the assumption that the SWCNTs are filled with water.[11] This filling is indeed possible, despite the hydrophobic nature and small diameter of SWCNTs, and has been the subject of many theoretical[12] and experimental studies.[13] In fact, high-resolution Raman spectroscopy of the radial breathing mode (RBM) vibration of SWCNTs has shown that both empty (closed) and water-filled (opened) SWCNTs occur in aqueous solutions,[5] and that SWCNTs can be filled down to extremely thin diameters ($d = 0.548$ nm).[14] Furthermore, it was shown that water-filled tubes dominate in solutions of chemically purified tubes or tubes that have been dispersed by using heavy ultrasonication,[5] as is almost universally applied in DGU work (even though also high concentrations of individual SWCNTs can be achieved using bile salt surfactants without ultrasound[3]).

Very importantly, the possible occurrence of empty tubes has not been taken into account in DGU separations, and we hypothesized that it would be beneficial to use intact, empty SWCNTs in DGU sorting for at least two reasons: 1) As the resolution in DGU separations is determined by the counteracting effects of gravity and diffusion, it improves with increasing molecular mass (for a given density),[8] and is therefore expected to be best for the empty SWCNTs (as these are end-capped, and therefore intact, full-length tubes). 2) A larger dependence of buoyant density on SWCNT diameter may be expected for empty tubes, at least for tubes with sufficiently large diameters where the volume of the internal (empty) channel plays a dominant role. The latter behavior can be qualitatively described by a very simple geometric model that treats the internal water molecules as hard spheres in a cylinder[15] and the surfactant as a concentric cylindrical layer around it (see Section 2 in the Supporting Information). This model results in a diameter dependence of the density which reverses at some intermediate diameter, but eventually, as intuitively expected, converges towards the density of water for large water-filled tubes, whereas it continues to decrease for empty tubes.

We first demonstrate that empty SWCNTs can be successfully separated from water-filled SWCNTs by DGU and that both species (empty and filled) can be further sorted by diameter in a single DGU run. To this end, we used SWCNTs synthesized by the arc-discharge method, which have a relatively large diameter d and narrow diameter distribution ($d = (1.33 \pm 0.1)$ nm). The SWCNTs were solubilized in D_2O with sodium cholate (SC) surfactant using only mild sonication to obtain solutions that contain both empty and water-filled SWCNTs. The solutions were first centrifuged at medium speed to remove any bundles so that only the individually solubilized SWCNTs remained. When such solutions were then ultracentrifuged in a gradient of iohexol[16] in D_2O, we observed a clear separation into two series of colored bands, which we collected into fractions labeled 1A–1D and 1E–1H (Figure 1a). High-resolution Raman spectra of these fractions (e.g., Figure 1c; analyzed by fitting the well-resolved peaks of empty and water-filled tubes by using the accurately determined peak positions and widths from Ref. [5]) showed that the lower-density fractions 1A–1D indeed contain only empty SWCNTs, whereas the higher-density fractions mainly contain water-filled SWCNTs (of the same chiral structures), and the original solution contained a mixture of both SWCNTs. The fact that colored bands are observed in both series already indicates that a separation of different SWCNT structures occurs among both empty and water-filled tubes. In fact, this observation also clearly excludes the fact that either series would correspond to remaining bundles or aggregates of SWCNTs[17] (which are actually found to band as a single, black band at even higher density when not removed beforehand; see the Supporting Information). Interestingly, this macroscopic separation evidently also implies that empty and water-filled tubes are largely present as fully separate entities, as opposed to the occurrence of empty and water-filled domains within the same nanotube (a behavior which could not be excluded from previous measurements on mixed samples[5,14]): any defect large enough to allow water molecules to pass causes the entire SWCNT to be water-filled. The structure separation is further supported by the absorption spectra (Figure 1b), which show a sequence of highly resolved features, especially within the range of the lowest-energy transition of the semiconducting SWCNTs at approximately 1500–1800 nm (not resolved in the original solution). As the wavelength of this transition is roughly related to diameter, the absorption spectra already hint at an opposite diameter–density relation among empty and water-filled tubes. However, the transition wavelengths of SWCNTs also depend to some extent on the exact chiral structure, and therefore more unequivocal information is obtained from 2D IR band-gap fluorescence excitation spectroscopy, which allows for resolving each individual SWCNT structure (identified by its chiral indices (n,m)).[18] An example of a 2D fluorescence map of a fraction of empty tubes is given in Figure 2a, and shows a band-gap emission that has a sharp peak at approximately 1550 nm (a technologically very important wavelength widely used, for example, in optical telecommunications). Three-color overlays of three empty SWCNT fractions of increasing densities (Figure 2b) and three water-filled SWCNT fractions of increasing density (Figure 2c) immediately show that 1) the optical transitions of the empty tubes are much more resolved (both in excitation and in emission) and 2) the sorting of SWCNT structures is based mainly on diameter and is influenced less by their chiral angle (compare with the superimposed diameter/chiral angle grid), but follows an order among empty and filled SWCNTs, with the largest diameter tubes at the lowest densities in the case of empty tubes (within the diameter range of these arc-discharge SWCNTs). This trend can be visualized more synoptically (similar to the absorption data, but with a more direct relation with diameter) by projecting the 2D fluorescence data along curves of constant diameter to obtain the 1D curves of fluorescence intensity as a function of diameter as shown in Figure 2f (see also Section 7 in the Supporting Information). Comparing 2D fluorescence maps for fractions of empty tubes with corresponding fractions of water-filled tubes (e.g., the two-color overlay in Figure 2d) reveals not only the dramatic broadening but also a significant red-shift of the electronic transitions induced by the water-filling, both in

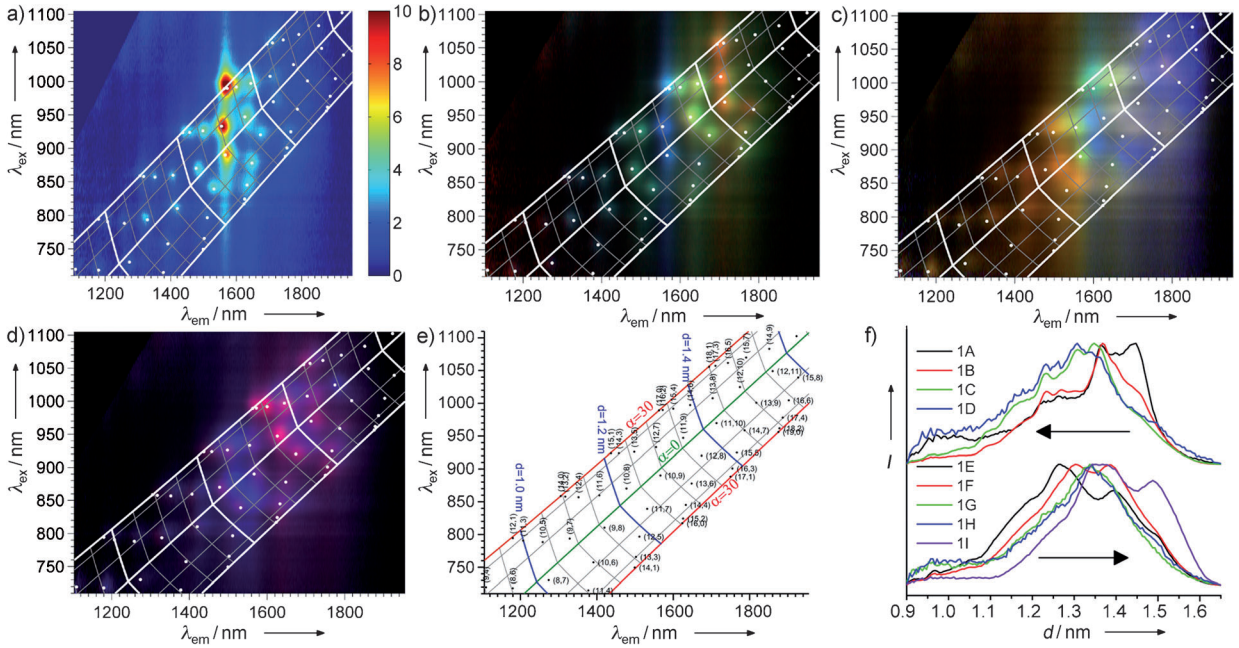

Figure 2. 2D IR fluorescence-excitation maps of fractions 1A–1I a) Example of a 2D IR fluorescence-excitation spectrum of fraction 1C, revealing the chirality distribution of the semiconducting tubes in this fraction. Empirical peak positions and a grid, visualizing the lines of constant density and chiral angle, are superimposed on the 2D spectrum. b) Three-color overlays of three empty fractions 1A (red; $\langle\rho\rangle = 1.163\ g\,mL^{-1}$), 1B (green; $\langle\rho\rangle = 1.175\ g\,mL^{-1}$), and 1C (blue; $\langle\rho\rangle = 1.182\ g\,mL^{-1}$), clearly revealing the diameter-based sorting for empty tubes. c) Three-color overlay of filled fractions 1E (red; $\langle\rho\rangle = 1.199\ g\,mL^{-1}$), 1F (green; $\langle\rho\rangle = 1.204\ g\,mL^{-1}$), and 1I (blue; $\langle\rho\rangle = 1.267\ g\,mL^{-1}$), showing the opposite diameter vs. density relation for filled tubes. d) Two-color overlay of fraction 1B (red) and fraction 1E (blue), evidencing the electronic red-shifts and broadening for water-filled SWCNTs. e) Labeled SWCNT peak positions (chiral indices (n,m)) and diameter/chiral angle grid over the same range as the 2D IR fluorescence spectra, all derived from the adapted empirical relations (Equation S2) for empty tubes. f) Integrated fluorescence intensity of the different fractions, integrated along strips of constant diameter, that reveal the opposite diameter versus density relation for empty (upper spectra) and filled SWCNTs (lower spectra).

excitation (second transition of semiconducting tubes E_{22}^S) and in emission (E_{11}^S).

To obtain a more detailed picture of the structure–density relation, we performed extensive resonance Raman and 2D fluorescence-excitation measurements, which both have the advantage of providing intensities (that are proportional to the concentrations, which were kept sufficiently low to avoid reabsorption) of each individual SWCNT structure present in the different fractions. This procedure allowed us to determine at which buoyant density each (empty and filled) tube structure (n,m) is concentrated (Figure 3). The result is in remarkable agreement with the qualitative predictions of the simple hard-sphere model, indeed showing a divergence between the densities of empty and water-filled tubes at increasing diameters, and the onset of the reversal of the diameter–density relation for empty SWCNTs. The Raman data also includes results for metallic SWCNTs, and shows that there are no significant density differences between metallic and semiconducting tubes of similar diameter. Superimposed on these general trends, significant oscillations are observed, which we attribute to packing effects of the surfactant molecules around SWCNTs of different diameters, which were already suggested to play an important role by Arnold et al.,[4a] and which can also help in the optimization of the separation of specific SWCNTs, albeit in a less predictable way, by using different surfactants, surfactant concentrations, or by adding electrolytes.[4a,d,h,19] In fact, it was

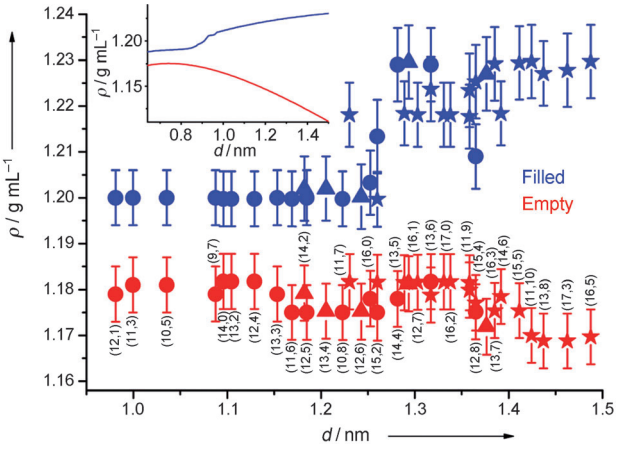

Figure 3. Density of empty and water-filled SWCNTs. Density of empty (red) and filled (blue) SWCNTs obtained from comparing resonance Raman intensities of semiconducting (circles) and metallic (triangles) tubes and IR fluorescence intensities (stars) of fractions 1A–1I. Error margins are determined by the density differences between subsequent fractions. Densities of fractions were determined from optical absorption spectrometry of the iohexol absorption at 2272 nm. The inset shows the calculated density vs. diameter relationship using the geometric model described in the Supporting Information.

recently found that reducing the surfactant concentration also improved the DGU-based sorting of thinner SWCNTs,[4c] which may be attributed to a reduction of the surfactant

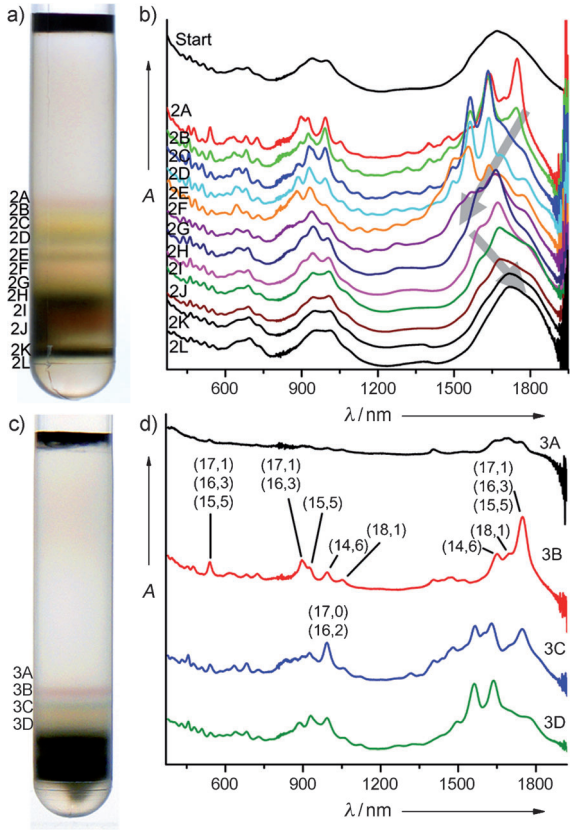

Figure 4. Sorting of Arc SWCNTs using 0.7% w/v SC. a) Centrifuge tube containing Arc SWCNTs sorted by a 24 h single DGU run at 122000 g in 0.7% w/v SC. Bands 2A–2E are empty SWCNTs, bands 2H–2J are water-filled tubes, and bands 2K–2L contain bundles. b) Absorption spectra of the unsorted and sorted fractions. Spectra are background-subtracted, normalized, and offset for clarity. c) Image of centrifuge tube containing Arc SWCNTs sorted by a 48 h single DGU run at 122000 g in 0.7% w/v SC. d) Absorption spectra of the sorted fractions showing very narrow chirality distributions. Indicated chiral indices are determined by combining absorption and fluorescence spectroscopy.

layer thickness (possibly from a double layer to a monolayer). Repeating our experiments with this lower surfactant concentration (0.7% SC; Figure 4) particularly enhances the oscillations (Figure 5b), which is consistent with the concept of a thinner surfactant layer that reduces the total volume and increasing the relative effect of the SWCNTs and of the surfactant monolayer packing on the effective buoyant density. These oscillations result in a more complex non-monotonous diameter sorting (Figure 5b,c), and help in the excellent sorting yielding only a few chiralities in separate fractions of empty tubes (see Figures 4c, 5a, and Figure S11 in the Supporting Information), but the same general trend is confirmed for an opposite diameter–density relation for empty and filled SWCNTs. Interestingly, use of a slightly different bile salt surfactant (sodium deoxycholate; DOC) results in much reduced oscillations and thus a more systematic general trend in the diameter–density relation that more clearly shows the opposite behavior for empty and filled tubes (see Figures S18–S20). While both bile salts are known to be very efficient surfactants (among which DOC is better than SC),[3] and both form a very homogeneous, unperturbing coating around the nanotubes, as indicated by the unusually narrow SWCNT spectral linewidths,[3] the present results show that slight variations of the structure of the surfactant (one extra OH group for SC), result in a different packing around the SWCNTs that is more critically dependent on the exact diameter in the case of SC, and is believed to be the dominant mechanism in the sorting of small-diameter SWCNTs (see the Supporting Information, Section 10).[4a]

The separation of empty and water-filled SWCNTs with a much wider diameter distribution, including thinner tubes (as produced by the high-pressure carbon monoxide (HipCO) process; $d \approx 0.7$–1.4 nm) at first seemed more challenging, as the buoyant density range of filled thin tubes may overlap with that of empty thicker tubes. This is indeed the case, but nevertheless we achieved a good separation of empty and water-filled tubes, both for the thinnest diameters (ca. 0.548 nm) and for the larger diameters (ca. 1.1 nm), especially when using DOC, which minimizes the surfac-

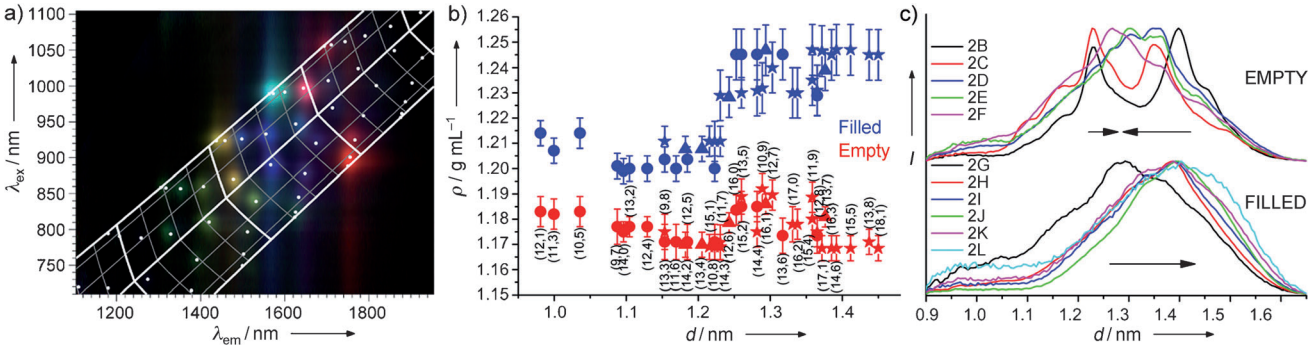

Figure 5. 2D IR fluorescence of sorted Arc SWCNTs using 0.7% w/v SC. a) Three-color overlay plot of the 2D IR fluorescence spectra of fractions 3B (red; $\langle\rho\rangle = 1.176\ g\,mL^{-1}$), 3C (green; $\langle\rho\rangle = 1.194\ g\,mL^{-1}$), and 3D (blue; $\langle\rho\rangle = 1.204\ g\,mL^{-1}$) clearly showing a very good sorting with only a few chiralities present in the fractions 3B and 3C. b) Density of empty (red) and filled (blue) SWCNTs obtained from comparing resonance Raman intensities of semiconducting (circles) and metallic (triangles) and IR fluorescence intensities (stars) of fractions 2A–2L. c) Integrated fluorescence intensities versus diameter for the fractions 2A–2L, showing the diameter-sorting and a turning point around 1.25 nm, which is attributed to the surfactant-induced fluctuation in the diameter–density relation.

tant-induced density modulation (see the Supporting Information).

The electronic and vibrational transitions of the SWCNTs, which are already extraordinarily sharp because of the very regular, unperturbing bile salt micellar coating,[3] are even narrower for the empty SWCNTs than for the water-filled SWCNTs.[5,14] Therefore, isolation of the empty SWCNTs results in solutions with by far the most resolved Raman spectra reported to date for carbon nanotubes (see for example, fraction 1B in Figure 1c and Section 5 and Figures S18 and S16 in the Supporting Information), with RBM linewidths as low as 1.16 cm^{-1} (e.g., the (6,4) tube in fraction 6B; see Figure S18d). This result implies very long phonon lifetimes (setting a lower limit of 4.6 ps for the empty (6,4) tube), which suggest improved thermal conductivities of these intact, empty SWCNTs. Also the electronic transitions are clearly much narrower (e.g., Figure 2 and Section 7 and Figures S3, S4, S14, and S19 in the Supporting Information), thus indicating that the electronic properties are much less perturbed. This result is indeed also confirmed by dramatically improved fluorescence efficiencies. A relative measure of fluorescence quantum efficiency is obtained by normalizing the fluorescence intensity to the absorbance (see the Supporting Information). The fluorescence quantum efficiency drops steeply with increasing diameter for both empty and water-filled tubes, but that of empty tubes is approximately twice as high as that of the more commonly used water-filled tubes. Likewise, the resonance Raman cross-section is found to be 4–5 times higher for the empty SWCNTs, which, when combined with the fact that the Raman scattering is also concentrated in much narrower RBM lines, results in extraordinarily strong peak intensities in Raman spectroscopy. Thus, all observations point at considerably enhanced electronic and vibrational (and thus thermal) properties for empty SWCNTs.

In conclusion, the fact that each SWCNT chirality may be observed at two different buoyant densities that correspond to empty and water-filled tubes, each of which has a different diameter–density relation, is not only essential to the understanding of the diameter-sorting process, but also provides an important new degree of freedom in the DGU separation of carbon nanotubes. It will be particularly important for the sorting of very large diameter SWCNTs to prepare these tubes in a pristine, closed (and therefore empty) state, as the density of water-filled tubes becomes essentially constant at large diameters. Moreover, the pristine empty tubes isolated by using this method not only have the largest possible aspect ratios but also display far more ideal, unperturbed properties than the filled tubes, as exemplified by the much narrower electronic and vibrational transitions and enhanced quantum efficiencies, and will thus be preferable in most applications.

Received: November 22, 2010
Published online: February 22, 2011

Keywords: carbon nanotubes · chirality · luminescence · surfactants · ultracentrifugation

[1] S. Iijima, T. Ichihashi, *Nature* **1993**, *363*, 603.
[2] S. Reich, C. Thompson, J. Maultzsch, *Carbon Nanotubes: Basic Concepts and Physical Properties*, Wiley-VCH, Weinheim, **2004**.
[3] W. Wenseleers, I. I. Vlasov, E. Goovaerts, E. D. Obraztsova, A. S. Lobach, A. Bouwen, *Adv. Funct. Mater.* **2004**, *14*, 1105.
[4] a) M. S. Arnold, A. A. Green, J. F. Hulvat, S. I. Stupp, M. C. Hersam, *Nat. Nanotechnol.* **2006**, *1*, 60; b) A. A. Green, M. C. Duch, M. C. Hersam, *Nano Res.* **2009**, *2*, 69; c) S. Ghosh, S. M. Bachilo, R. B. Weisman, *Nat. Nanotechnol.* **2010**, *5*, 443; d) P. Zhao, E. Einarsson, R. Xiang, Y. Murakami, S. Maruyama, *J. Phys. Chem. C* **2010**, *114*, 4831; e) M. C. Hersam, *Nat. Nanotechnol.* **2008**, *3*, 387; f) J. Liu, M. C. Hersam, *MRS Bull.* **2010**, *35*, 315; g) R. Fleurier, J. S. Lauret, U. Lopez, A. Loiseau, *Adv. Funct. Mater.* **2009**, *19*, 2219; h) Y. Kato, Y. Niidome, N. Nakashima, *Angew. Chem.* **2009**, *121*, 5543; *Angew. Chem. Int. Ed.* **2009**, *48*, 5435.
[5] W. Wenseleers, S. Cambré, J. Čulin, A. Bouwen, E. Goovaerts, *Adv. Mater.* **2007**, *19*, 2274.
[6] M. S. Arnold, S. I. Stupp, M. C. Hersam, *Nano Lett.* **2005**, *5*, 713.
[7] J. A. Fagan, M. L. Becker, J. Chun, E. K. Hobbie, *Adv. Mater.* **2008**, *20*, 1609.
[8] C. A. Price, *Centrifugation in Density Gradients*, Academic Press, New York, **1982**.
[9] A. G. Rinzler, *Nat. Nanotechnol.* **2006**, *1*, 17.
[10] N. Nair, W. J. Kim, R. D. Braatz, M. S. Strano, *Langmuir* **2008**, *24*, 1790.
[11] a) M. S. Arnold, J. Suntivich, S. I. Stupp, M. C. Hersam, *ACS Nano* **2008**, *2*, 2291; b) A. Quintillá, F. Hennrich, S. Lebedkin, M. M. Kappes, W. Wenzel, *Phys. Chem. Chem. Phys.* **2010**, *12*, 902; c) E. J. F. Carvalho, M. C. dos Santos, *ACS Nano* **2010**, *4*, 765.
[12] a) K. Koga, G. T. Gao, H. Tanaka, X. C. Zeng, *Nature* **2001**, *412*, 802; b) A. Alexiadis, S. Kassinos, *Chem. Rev.* **2008**, *108*, 5014.
[13] a) G. Hummer, J. C. Rasaiah, J. P. Noworyta, *Nature* **2001**, *414*, 188; b) J. K. Holt, *Microfluid. Nanofluid.* **2008**, *5*, 425.
[14] S. Cambré, B. Schoeters, S. Luyckx, E. Goovaerts, W. Wenseleers, *Phys. Rev. Lett.* **2010**, *104*, 207401.
[15] G. T. Pickett, M. Gross, H. Okuyama, *Phys. Rev. Lett.* **2000**, *85*, 3652.
[16] a) D. Rickwood, T. Ford, J. Graham, *Anal. Biochem.* **1982**, *123*, 23; b) The use of iohexol, which has a lower molecular weight than the more commonly used iodixanol, as well as the use of D_2O instead of H_2O, allows for the creation of shallower and more stable gradients.
[17] J. Crochet, M. Clemens, T. Hertel, *J. Am. Chem. Soc.* **2007**, *129*, 8058.
[18] S. M. Bachilo, M. S. Strano, C. Kittrell, R. H. Hauge, R. E. Smalley, R. B. Weisman, *Science* **2002**, *298*, 2361.
[19] a) S. Niyogi, C. G. Densmore, S. K. Doorn, *J. Am. Chem. Soc.* **2009**, *131*, 1144; b) F. Bonaccorso, T. Hasan, P. H. Tan, C. Sciascia, G. Privitera, G. Di Marco, P. G. Gucciardi, A. C. Ferrari, *J. Phys. Chem. C* **2010**, *114*, 17267.

Angewandte Chemie
Eine Zeitschrift der Gesellschaft Deutscher Chemiker

Supporting Information

69451 Weinheim, Germany

Separation and Diameter-Sorting of Empty (End-Capped) and Water-Filled (Open) Carbon Nanotubes by Density Gradient Ultracentrifugation**

*Sofie Cambré and Wim Wenseleers**

anie_201007324_sm_miscellaneous_information.pdf

TABLE OF CONTENTS

1. Materials and Methods

2. Geometric model for the density of empty and water-filled SWCNTs

3. Spectral shifts in the absorption of empty and water-filled SWCNTs

4. Raman spectra excited at different wavelengths

5. Raman cross-section of empty and water-filled SWCNTs

6. Adapted empirical relations for the SWCNT electronic transition energies

7. Band-gap fluorescence-excitation maps of sorted DGU fractions and data analysis

8. Relative fluorescence quantum efficiency of empty and water-filled SWCNTs

9. DGU sorting with 2% w/v DOC (Arc SWCNTs)

10. Separation of empty and water-filled HipCO SWCNTs, with SC *vs*. DOC

1. Materials and Methods

Solubilization. Raw SWCNTs synthesized by the arc-discharge method (Arc, *d*=[1.33 ± 0.1]nm) were obtained from Nanoledge (batch #F00508D). Two bile salts, sodium cholate[1] (SC, 99%) and sodium deoxycholate[1] (DOC, also referred to as SDC in the literature, 99%) were used as surfactants and were both obtained from Acros organics. D_2O was obtained from CorTecNet (99.89% atomD). 10 mg of SWCNTs were added to 3 mL of a 1%w/v surfactant solution in D_2O. D_2O is mainly used for its optical transparency in the IR, as required for the spectroscopic characterization (absorption, band-gap fluorescence) of these larger diameter tubes, and its higher density is also beneficial in the centrifugation (see below). The solution was stirred for several days and afterwards sonicated for 15 min in a bath sonicator (BRANSONIC, 1510E-MTH, 70W, 42kHz), in order to obtain sample solutions with (only) a fraction of opened (water-filled) tubes.[2] More sonication, or sonication from the very start of the solubilization process, results in a too high fraction of opened tubes which is undesirable for our purposes. Then the solution was centrifuged at 16215g (Sigma 2-16KCH centrifuge with swing-out rotor, 14000 rpm), in order to sediment out nanotube aggregates and bundles and end up with individually isolated SWCNTs in solution. This first medium speed "pre-centrifugation" is based on sedimentation rate, rather than density, and is not strictly necessary, but avoids very dense aggregate bands below the bands of the water-filled tubes in the subsequent ultracentrifugation (e.g. visible in the less thoroughly pre-centrifuged samples 5-7), the tails of which may overlap with these water-filled SWCNT bands (e.g. although bundles of SWCNTs possess higher densities than individual tubes, aggregates of entangled [empty and water-filled] tubes may have intermediate densities, but can still be separated based on sedimentation speed). The same solubilization procedure was used for raw HipCO SWCNTs (batch #R0495C, Carbon Nanotechnologies Inc.), spanning a diameter range from 0.7-1.4 nm, except that no sonication was used during the solubilization.

Density Gradients. The density gradient medium used throughout this study is iohexol (5-(*N*-2,3-dihydroxypropylacetamido)-2,4,6-triiodo-*N,N'*-bis(2,3-dihydroxypropyl)isophthalamide).[3] Iohexol (tradename "NycoDenz") was obtained from Axis-Shield in powder form, and dissolved in D_2O at appropriate concentrations to obtain the desired density ranges, as detailed below. Iohexol is a monomeric analogue of the more commonly used dimer iodixanol. While allowing similar densities to be achieved, the lower molecular weight of iohexol makes it less sensitive to redistribution under the influence of the centrifugal field – a common limitation in maintaining shallow gradients during strong and/or prolonged ultracentrifugal separations.[4] The use of D_2O further helps in creating shallow, stable gradients, as the higher density of D_2O allows the required density to be reached with lower mass-fractions of gradient medium added. These gradients also possess extremely low viscosities.

Gradients were prepared in 1.3 mL polyallomer centrifuge tubes by starting from a step gradient (low density layer added gently on top of a higher density layer) and then tilting the tube ~80° and rolling it around its axis to form a continuous gradient. Then the SWCNT solution was added on top of the gradient, or (for samples 5-6) included directly in the upper half of the gradient. In all three layers the surfactant concentration was adjusted to the same value (0.7%w/v or 2%w/v). For the specific samples shown in the figures the following compositions were used:

Sample 1 (Fig. 1a): Bottom layer: 0.6 mL, ρ=1.27 g mL^{-1}; 34%w/v iohexol; 2% w/v SC in D_2O
Middle layer: 0.6 mL, ρ=1.158 g mL^{-1}; 11%w/v iohexol; 2% w/v SC in D_2O
Top layer: 0.1 mL Arc SWCNT solution (24h pre-centrifugation); 2%w/v SC in D_2O

Sample 2 (Fig. 4a): Bottom layer: 0.55 mL, ρ=1.27 g mL^{-1}; 34%w/v iohexol; 0.7% w/v SC in D_2O
Middle layer: 0.55 mL, ρ=1.145 g mL^{-1}; 8%w/v iohexol; 0.7% w/v SC in D_2O
Top layer: 0.2 mL Arc SWCNT solution (24h pre-centrifugation); 0.7%w/v SC in D_2O

Sample 3 (Fig. 4c): Bottom layer: 0.5 mL, ρ=1.22 g mL^{-1}; 24%w/v iohexol; 0.7% w/v SC in D_2O
Middle layer: 0.5 mL, ρ=1.158 g mL^{-1}; 11%w/v iohexol; 0.7% w/v SC in D_2O
Top layer: 0.3 mL Arc SWCNT solution (24h pre-centrifugation); 0.7%w/v SC in D_2O

Sample 4 (Fig. S14): Bottom layer: 0.6 mL, ρ=1.30 g mL^{-1}; 41%w/v iohexol; 2% w/v DOC in D_2O
Middle layer: 0.6 mL, ρ=1.134 g mL^{-1}; 6%w/v iohexol; 2% w/v DOC in D_2O
Top layer: 0.1 mL Arc SWCNT solution (24h pre-centrifugation); 2%w/v DOC in D_2O

Sample 5 (Fig. S16): Bottom layer: 0.6 mL, ρ=1.27 g mL^{-1}; 34%w/v iohexol; 0.7% w/v SC in D_2O
Top layer: 0.7 mL, ρ=1.145 g mL^{-1}; 8%w/v iohexol; HipCO SWCNTs (1h pre-centrifugation); 0.7% w/v SC in D_2O

Sample 6 (Fig. S18): Bottom layer: 0.6 mL, ρ=1.27 g mL^{-1}; 34%w/v iohexol; 0.7% w/v DOC in D_2O
Top layer: 0.7 mL, ρ=1.186 g mL^{-1}; 16%w/v iohexol; HipCO SWCNTs (1h pre-centrifugation); 0.7% w/v DOC in D_2O

Sample 7 (Fig. S7): Bottom layer: 0.6 mL, ρ=1.340 g mL^{-1}; 49%w/v iohexol; 2% w/v SC in D_2O
Middle layer: 0.6 mL, ρ=1.176 g mL^{-1}; 15%w/v iohexol; 2% w/v SC in D_2O
Top layer: 0.1 mL HipCO SWCNT solution (1h pre-centrifugation); 2%w/v SC in D_2O

Ultracentrifugation was performed using a centrifuge (Kontron Centrikon T-1080) with swing-out rotor (TST 28), operated at 20°C. The solutions were centrifuged for 24h (samples 1, 2, 4 and 7) or 48h (samples 3, 5, and 6) at 28000 rpm (122.000g max.). After centrifugation, the different coloured bands were fractionated manually from top to bottom using a syringe. Note that the diameter separations in this work are achieved despite the relatively low centrifugation speeds used (compared to the accelerations of ~200.000 *g* or even more[4b, 5] often used in literature). As the resolution of separation in DGU (i.e. the widths of the bands corresponding to individual species) is determined by the balance between gravity and diffusion, this resolution (at equilibrium) essentially scales with the acceleration (neglecting any pressure-induced changes in the surfactant coating[4a, 6]), and the time to reach this equilibrium is reduced accordingly. Thus a corresponding further improvement can be expected when using higher speed centrifuges.

Characterization of sorted SWCNT samples: Absorption spectroscopy. Absorption spectra were collected using a Varian Cary 5E UV-VIS-IR spectrometer in the range of 200-2500nm, using quartz (micro-)cells with appropriate path lengths (0.1, 1 or 3 mm). To determine the densities of the different fractions (iohexol concentrations), the absorption peak of iohexol at 2272 nm was used, which was calibrated against several solutions of known concentration and density. For characterization of the SWCNTs, absorption spectra were corrected for the absorption of the surfactant, D_2O (and trace H_2O impurities) and the density gradient medium. Furthermore, for display in the figures, a 1/wavelength background was subtracted,[7] and the absorption spectra were rescaled, and vertically offset for clarity.

Characterization of sorted SWCNT samples: resonant Raman spectroscopy. Raman spectra were recorded in backscattering geometry using a Dilor XY800 triple spectrometer with liquid nitrogen cooled CCD detection. Several excitation wavelengths from three different lasers (Ar^+, Kr^+, Ti:sapphire) were used. For a first characterization of the samples solubilised using DOC, a wavelength of 785nm was used (Ti:sapphire laser), in resonance with the (12,1), (11,3), (10,5) and (9,7) tubes, for which the Raman peak positions and linewidths of the empty and water-filled tubes were already very accurately known from reference [2], allowing a straightforward fit of the spectra with a linear combination of these known (Lorentzian) peaks. The same procedure was used for the thin tubes ((6,5), (6,4), and (7,2)) excited at 568nm (Kr^+ laser), using the more extensive data from reference [8] (and the corresponding EPAPS documents). For other wavelengths, the Raman spectra of all sorted fractions originating from one sample were simultaneously fitted using for each SWCNT (*n*,*m*) chirality, a sum of two Lorentzians, corresponding to empty and water-filled SWCNTs, following the same procedure as in references [2,8]. This simultaneous fitting procedure yields very reliable positions and linewidths, also for chiralities which were difficult to resolve in previous work[8] (such as the metallic tubes excited at 647.1nm), because the DGU sorted fractions used in the present work also include solutions containing exclusively empty SWCNTs. For samples with a different surfactant (SC instead of DOC) or surfactant concentration (0.7%w/v vs. 2%w/v) the peak positions and linewidths were allowed to vary, but both remained essentially the same (difference in position $<< 1$ cm^{-1}). The Raman signal of the density gradient medium and/or the plasma lines of the laser, when present, were included in the fitting procedure. Note that for some of the bottom (highest density) fractions (fractions 2K and 2L in Figure S6), also bundles are present, which causes both the electronic transitions to shift and broaden – bringing other tubes into resonance – as well as the RBM vibrational peaks to broaden. As a result, the Raman spectra of these bottom fractions cannot be fitted reliably, but were shown just for completeness (showing mainly that the overall Raman intensity of these fractions is very weak). This shift and broadening was most obvious for thin tubes (e.g. (8,3) and (9,1); not shown).

Characterization of sorted SWCNT samples: 2D IR fluorescence. 2D IR band-gap fluorescence-excitation spectra were recorded using a home-built dedicated set-up: The sample was excited using a pulsed Xe-lamp (Edinburgh Instruments, Xe900/xP920) with a 300 mm grating monochromator (Acton SpectraPro 2355). Emission was collected at 90° and analysed using a 150 mm grating spectrograph (Acton SpectraPro 2156) with a liquid nitrogen cooled extended InGaAs photodiode array detector (Princeton Instruments OMA V:1024/LN-

2.2), sensitive up to 2.2 µm. Spectra were recorded with 5nm steps in excitation wavelength, and an instrumental resolution of ~8 nm in excitation and ~20 nm in emission wavelength. Appropriate filters were used to eliminate stray light and higher order diffractions from the spectrometers, and all spectra were corrected for detector and spectrograph efficiency, filter transmission, and (temporal and spectral) variations of the excitation light intensity.

2. Geometric model for the density of empty and water-filled SWCNTs

In order to qualitatively describe the expected general trend of buoyant density with increasing diameter for empty and water-filled SWCNTs, we implemented a very simple geometric model. Building further on such a model by Quintilla *et al.*[9], we can approximate the buoyant density of a SWCNT coated with a surfactant layer by that of concentric cylindrical shells (See also Figure S1):

$$\rho = \frac{\rho_{\mathrm{int}}\left(d_{NT} - d_{wall}\right)^2 + \rho_{wall}\left(\left(d_{NT} + d_{wall}\right)^2 - \left(d_{NT} - d_{wall}\right)^2\right) + \rho_{surf}\left(\left(d_{NT} + d_{wall} + 2d_{surf}\right)^2 - \left(d_{NT} + d_{wall}\right)^2\right)}{\left(d_{NT} + d_{wall} + 2d_{surf}\right)^2} \qquad \text{(S1)}$$

with ρ_{int} the density of the internal channel (=0 for empty tubes), ρ_{wall} the density of the SWCNT wall, which can be approximated by the density of graphite ρ_{wall} = 2.23 g mL^{-1}, and ρ_{surf} the density of the surfactant layer. d_{NT} is the diameter of the SWCNT which is defined, as usual, from carbon nucleus to carbon nucleus, d_{wall} the thickness of the SWCNT wall, which we approximated by the van der Waals diameter of carbon, d_{wall} = 0.34 nm. The surfactant layer was approximated as a cylindrical shell with density ρ_{surf} = 1.0 g mL^{-1} and thickness d_{surf} corresponding to a single layer of cholate molecules, which was estimated from a molecular model to be d_{surf} = 0.7 nm, in line with estimates in literature in the range of 0.5-0.85 nm.[9-10] Alternatively, in literature the number of surfactant molecules adsorbed on the SWCNTs has also been estimated by fitting to experimental data,[4a, 10a, c] but this has only been done for a few SWCNT chiralities – not for the diameters used in the present study.

For water-filled SWCNTs, also the internal water molecules should be taken into account. As a first approximation one could set ρ_{int} in equation (S1) to a constant value equal to the density of bulk water ρ_{water} as was done in [10a] (in our case we used D_2O, so ρ_{water} = 1.105 g mL^{-1}). However, for the diameters considered here, comparable to the size of water molecules, the encapsulated row(s) of water molecules are not expected to be well described by a continuum model. Instead, one could estimate the number density of water molecules inside the tubes from molecular dynamics simulations for specific tube chiralities.[9, 10b] However, a qualitative but general picture of the diameter dependence of the internal water density can also be obtained by simply approximating the water molecules by hard spheres, closely packed in a hard cylinder, a mathematical problem which has been tackled analytically by Pickett *et al.*[11] (for cylinder diameters up to 2.155 times the sphere diameter). They found that depending on the diameter of the cylinder, different chiral phases of the spherical particles are formed, similar to what is found in far more elaborate theoretical calculations for water molecules inside specific SWCNTs.[12] As the diameter of a water molecule to be used in this hard-sphere approximation,

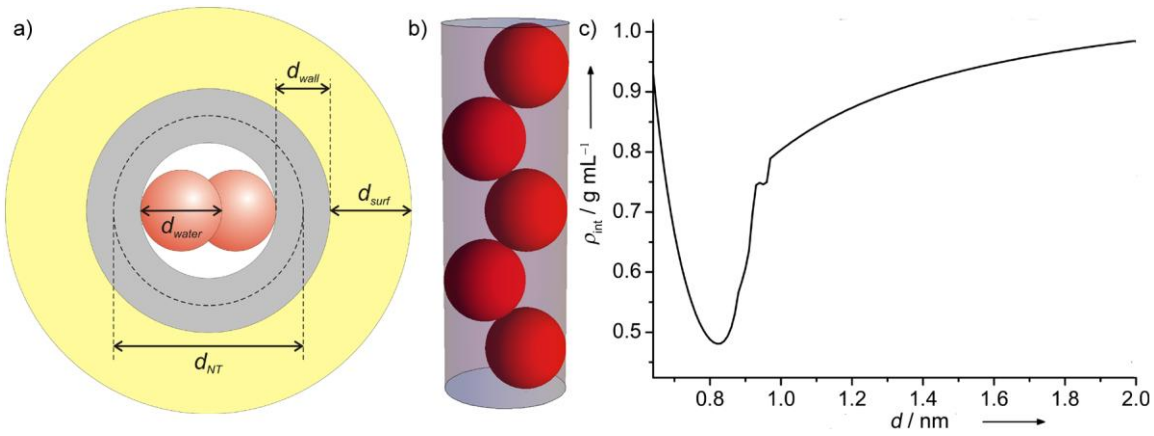

Figure S1: Geometrical model of a water-filled, surfactant-coated SWCNT. a) Schematic representation of a SWCNT with diameter d_{NT} and wall thickness d_{wall}. The surfactant layer is treated as a concentric cylindrical shell with thickness d_{surf}, and the internal water molecules are approximated by hard spheres with diameter d_{water}. b) One of the phases occurring for the hard spheres close-packed in the cylindrical internal channel, as described by Pickett *et al.*[11] (shown here for a diameter of the internal channel of $d_{NT} - d_{wall} = 1.5 \times d_{water}$) c) Density of the water-filled cylindrical inner channel, ρ_{int}, as obtained from the hard-sphere model (continuously interpolated at large diameters).

we used d_{water} =0.29 nm, the distance between the oxygen nuclei of two water molecules when they are connected by a hydrogen bond. For diameters larger than those for which analytical results have been obtained in reference [11], the volume fraction of the hard-sphere packing was extrapolated as $a+b/d$, such that at infinite diameter d, the volume fraction of a bulk close packing of spheres, $a = \pi/3\sqrt{2}$, is retrieved. The density of the spheres was chosen such that this bulk close-packed arrangement corresponds to the density of bulk water. The density of the water-filled cylindrical inner channel, as obtained from this hard-sphere model, is shown in Figure S1c. As expected, it yields a high filling density for tube diameters which just fit a single row of molecules, but drops to a pronounced minimum for slightly larger diameters, in line with the minimum in the water-filling induced shift of the RBM frequency of SWCNTs (corresponding to a minimum of the internal water counter-pressure) which was observed experimentally for SWCNT diameters of ~0.9 nm.[8]

The results of this simple geometric model for the buoyant density of surfactant coated SWCNTs are plotted in Figure S2. The red curve shows the evolution of density with diameter for empty SWCNTs: For very small diameters, the density of empty SWCNTs increases with diameter, due to the decreasing volume fraction of the (lower density) surfactant layer relative to the volume of the SWCNT wall. For larger diameter SWCNTs the density decreases with increasing diameter, as the influence of the empty internal volume starts to dominate. For water-filled tubes (blue curve in Figure S2), the density continues increasing up to larger diameters, eventually converging towards the density of bulk water, yielding a nearly diameter independent density for larger diameters. Of course, considering the very crude approximations and large uncertainties on the parameters involved in this model, no quantitative agreement with experiment can be expected (e.g. on the exact diameter at which the maximum buoyant density is reached etc.). Nevertheless, this simple model seems to capture the essence of the effects determining the diameter-density relation, explaining the origin of the observed general trends, with densities of empty and filled tubes diverging with increasing diameter, and empty

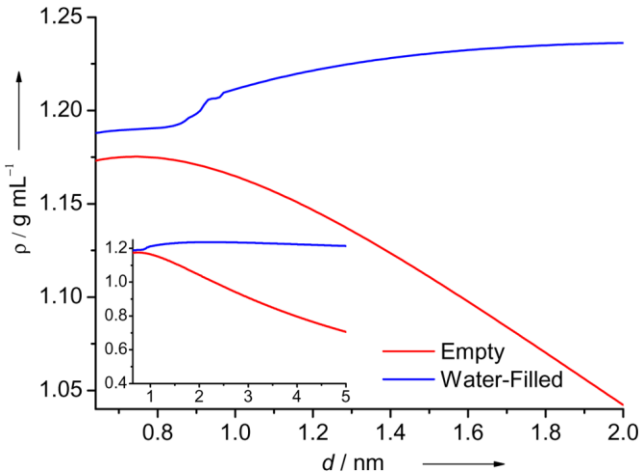

Figure S2: Model curves for the density of empty and water-filled SWCNTs. Calculated density for empty (red) and water-filled (blue) SWCNTs using the geometrical model described in this section and depicted in Figure S1a. The inset shows the same curves over a wider diameter range.

tubes showing a reversed diameter-density relation. Also, it becomes evident that for larger diameter SWCNTs a better separation can be expected using empty (closed) SWCNTs. Indeed, when using 0.7%w/v surfactant, very good isolation of only a few chiralities can be achieved. One important aspect which is *not* included in the model, is the packing of the discrete (and quite large, semi-rigid) bile salt surfactant molecules on the 2D SWCNT surface, which may e.g. lead to significant saw-tooth-like oscillations of the buoyant density depending on the commensurability of the packing with the circumference of the tubes. Even though the experimentally observed density oscillations seem, at first sight, similar to the effect of the internal water density of Figure S1c, they occur at significantly larger diameters, and we rather ascribe these oscillations (at least in part) to the surfactant packing effects. Indeed, the oscillations are highly dependent on both the type (SC or DOC) and concentration of surfactant. At small diameters (as used in most DGU separations in literature) the general variation of density with diameter as predicted by the present model is very weak, and therefore such surfactant packing effects are likely to dominate the DGU sorting process at small diameter, as pointed out by Arnold *et al.*[4b].

3. Spectral shifts in the absorption of empty and water-filled SWCNTs

After separating empty and water-filled SWCNTs, highly resolved absorption spectra are obtained, even for the large diameters of Arc SWCNTs – in fact yielding the most resolved absorption spectra of such large diameter SWCNTs observed to date.[1, 4b, 13] This allows us to look for shifts of these narrow features. Comparing absorption spectra of separated empty SWCNT solutions with corresponding water-filled SWCNTs, immediately reveals that the electronic resonances of the water-filled SWCNTs are systematically red-shifted with respect to those from the empty SWCNTs. For instance, Figure S3 shows the absorption spectra of an empty fraction of sample 1 (2%w/v SC) and a corresponding filled fraction. Some of the red-shifts are indicated in the figure, and are within the range of 10-30 meV. These shifts are also observed (Figure S4) when comparing the absorption spectrum of a DGU fraction containing *all* empty SWCNTs and a fraction containing

all filled SWCNTs from a given starting solution (i.e. from a DGU run as shown in Figure 4a in the main text – 0.7%w/v SC, but combining fractions 2A-2F and 2G-2L respectively). These red-shifts are in very good agreement with the red-shifts which we previously observed for 6 specific semiconducting tube chiralities through tuneable wavelength resonant Raman scattering experiments on mixed samples.[2, 8] The present absorption spectra show that these water-filling induced red-shifts are very general, and occur both for metallic

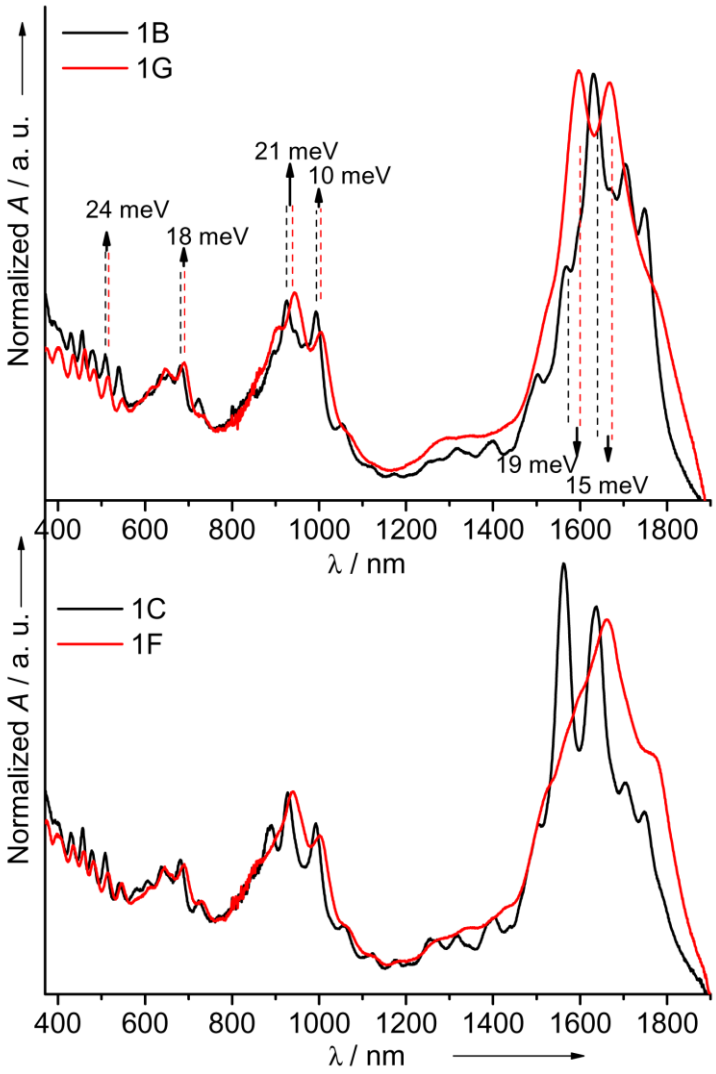

Figure S3: Absorption spectra of DGU sorted empty and water-filled SWCNTs. Normalized absorption spectra of fractions 1B and 1C (empty, black), compared with those of fractions 1G and 1F (water-filled, red) respectively, as obtained after sorting with 2%w/v SC. Some of the red-shifts of resonances of water-filled SWCNTs relative to the empty ones are indicated.

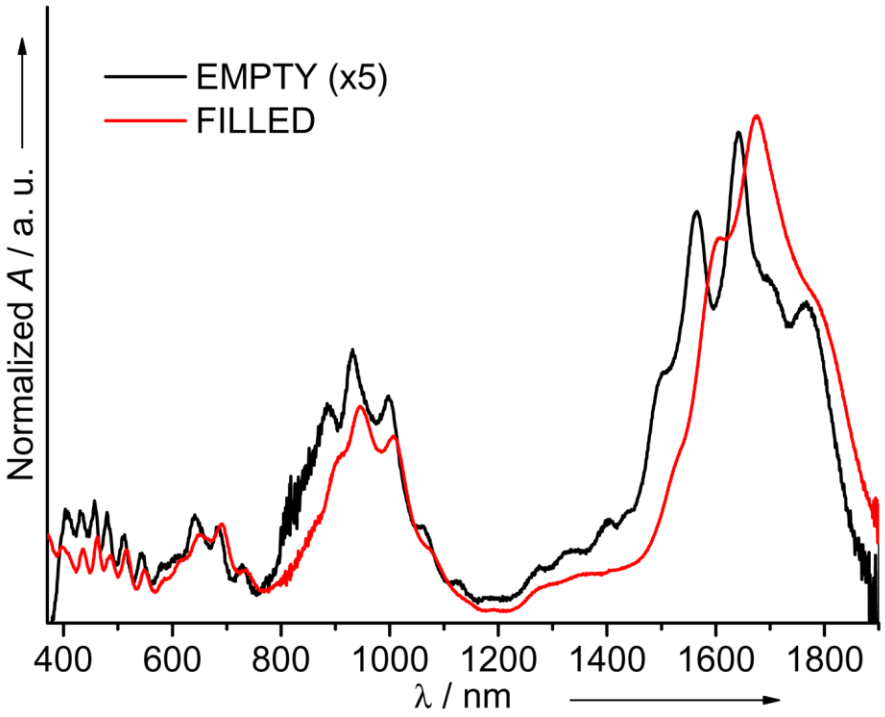

Figure S4: Spectra of DGU sorted empty and water-filled SWCNTs. Absorption spectra of the combination of all empty (black) and all water-filled (red) SWCNTs (sorted with 0.7% w/v SC), clearly showing the red-shift for water-filled SWCNTs.

tubes (first electronic resonance in the range of ~580-750nm) as well as for all of the observed transitions (first = band-gap, second, and third) of the semiconducting tubes. These red-shifts are also systematically observed for the smaller diameter HipCO SWCNTs (which always yield more resolved absorption spectra due to the smaller and therefore wider-spaced diameters; see Section 10, Figure S18c). More detailed information on these internal water induced red-shifts, resolving each of the individual semiconducting SWCNT chiralities, is also obtained from 2D fluorescence-excitation spectroscopy (see Sections 7-8).

4. Raman spectra excited at different wavelengths

Using resonant Raman scattering excited at different wavelengths, we were able to probe the density profile of 28 different nanotube chiralities (present in the Arc and HipCO SWCNT solutions combined), in the different fractions after DGU sorting. Resonant Raman spectroscopy is an extremely important characterization technique as it not only allows each individual SWCNT chirality to be identified, but moreover allows the resonances of empty and water-filled SWCNTs to be resolved: The water-filling of SWCNTs leads to an up-shift of the RBM frequency combined with a broadening of the resonance lines.[2, 8] Through many experiments on an extensive range of SWCNT samples treated in various chemical and/or mechanical ways to open/close them, the RBM peaks (position and linewidth) of empty (closed) and water-filled (open) SWCNTs have been unambiguously identified and characterised.[2, 8] For instance, it was shown that this up-shift can only be

ascribed to filling of the tubes and not to e.g. the presence of bundles.[2, 8] The latter is also further confirmed in the present work, as the water-filled tubes also show a clear diameter sorting after DGU, which would not be possible if the tubes were aggregated or entangled. Indeed, DGU of samples which have been subjected to a less thorough pre-centrifugation (samples 5-7) show bundles accumulating as a black band at even higher densities. In fact, the present DGU results moreover show that the empty and water-filled tubes coexist as clearly separate species in a solution, rather than empty and water-filled domains occurring in the same SWCNT. This means that once a defect (such as a missing end-cap) large enough to pass a water molecule is present, the entire nanotube is filled.

By using different laser wavelengths, different subsets of SWCNT chiralities, in resonance with this wavelength, are probed. In Figures S5 and S6 we give an overview of the different RRS spectra and fits (using a sum of two Lorentzians for each SWCNT chirality (*n*,*m*), corresponding to empty and water-filled SWCNTs, as in references [2, 8]), for DGU sorted fractions of Arc SWCNTs dissolved in 2%w/v and 0.7%w/v surfactant. Note that even within a single series of Raman spectra obtained at a single wavelength, only probing a subset of SWCNTs with very similar diameters, the diameter sorting can be observed as the relative intensities of the different peaks in the different fractions vary accordingly. The absolute intensities of each of the Lorentzian peaks were used to determine the density at which each empty and water-filled SWCNT species is most concentrated, resulting in the data shown in Figures 3 and 5b in the main text, and in Figures S17 and S20. Unique to RRS is that also the sorting for the metallic tubes can be observed (Figure S5b and S6b, and summarising Figures 3, 5b, S17, and S20), which are not visible in 2D IR fluorescence spectroscopy.

5. Raman cross-section of empty and water-filled SWCNTs

Measuring resonant Raman spectra of the DGU separated empty and water-filled SWCNTs, we immediately noticed that the empty SWCNT fractions yielded surprisingly intense Raman signals. To quantify this effect, we normalized the Raman spectra of the empty and water-filled SWCNT fractions (separated in 0.7% w/v SC) over their absorbance at the corresponding excitation wavelengths. We then compared the integrated intensities of these Raman spectra. For the tubes excited at 647.1 nm (metallic SWCNTs) we found that the Raman cross-sections of empty ones are a factor of 4.0 larger than for the water-filled ones. For the tubes excited at 501.7 nm and 855 nm (semiconducting SWCNTs), respectively, a factor of 5.2 and 4.2 was found. As the RBM peaks are also narrower for empty than for water-filled tubes,[2, 8] this implies that the peak intensities (as opposed to the aforementioned integrated intensities) of the empty tubes are enhanced by an even larger factor.

Note that this difference in Raman cross-section between empty and water-filled tubes also has important implications to the use of Raman spectroscopy in quantifying (relative or absolute) SWCNT concentrations, as both empty and water-filled SWCNTs commonly coexist in the same solutions, at widely varying ratios.[2, 8] For instance, we previously found that apparently benign operations such as bath ultrasonication or even simply stirring a SWCNT solution can already damage and water-fill a large fraction of the SWCNTs, as observed by

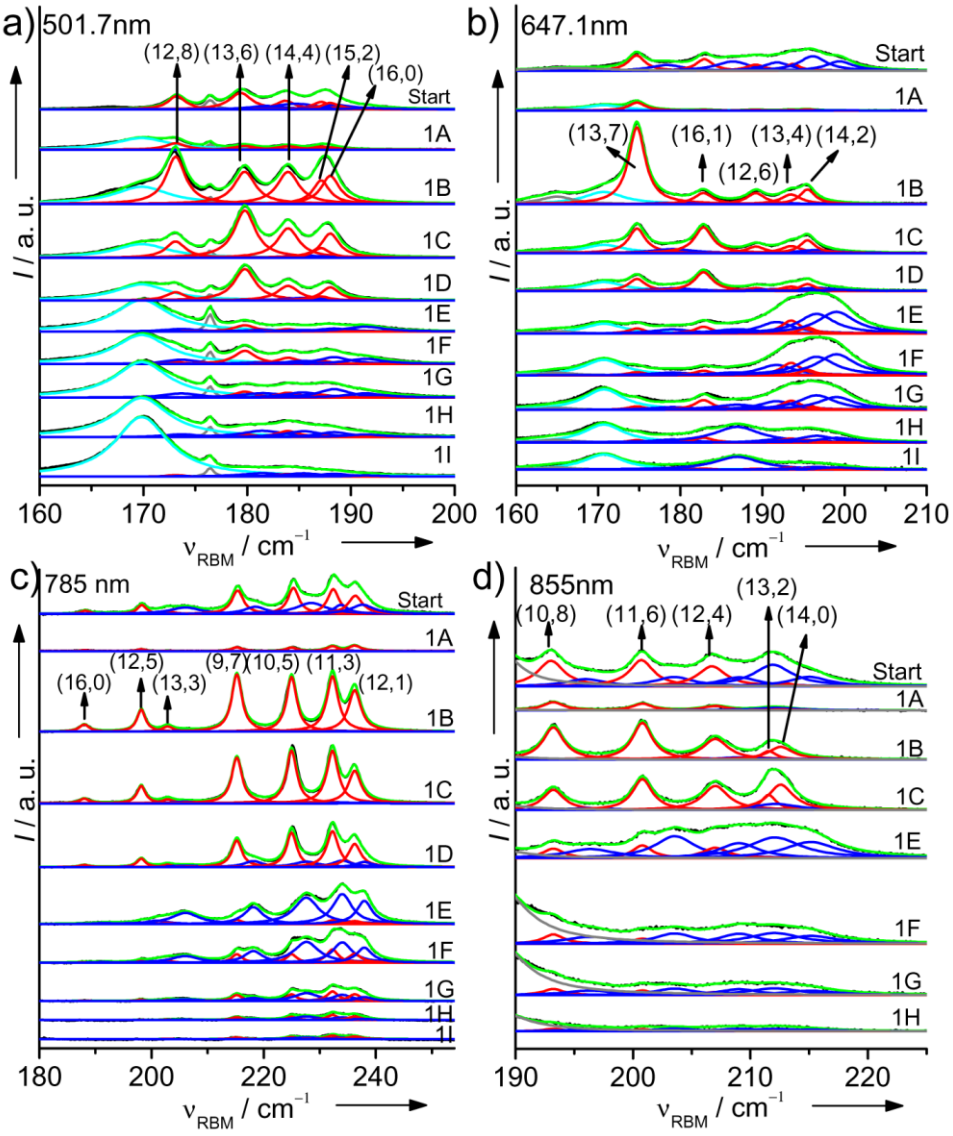

Figure S5: Resonant Raman spectra and fits of fractions 1A-1I (2%w/v SC) excited at different wavelengths. RRS spectra (black) are presented together with their best fits (green), composed of two Lorentzians for each SWCNT chirality (*n*,*m*), corresponding to empty (red) and water-filled (blue) SWCNTs. A Raman band of the gradient medium (cyan), when present, is also implemented in the fit. a) For excitation at 501.7 nm, in the third optical transition of the semiconducting tubes. Also a contribution from a plasma line of the laser (gray) is fitted. b) Excitation at 647.1nm, in the first optical transition of the metallic tubes. c) Excitation at 785 nm, in the second optical transition of the semiconducting tubes. d) Excitation at 855nm, in the second optical transition of semiconducting tubes. The gray curve in the fit corresponds to tubes further out of resonance.

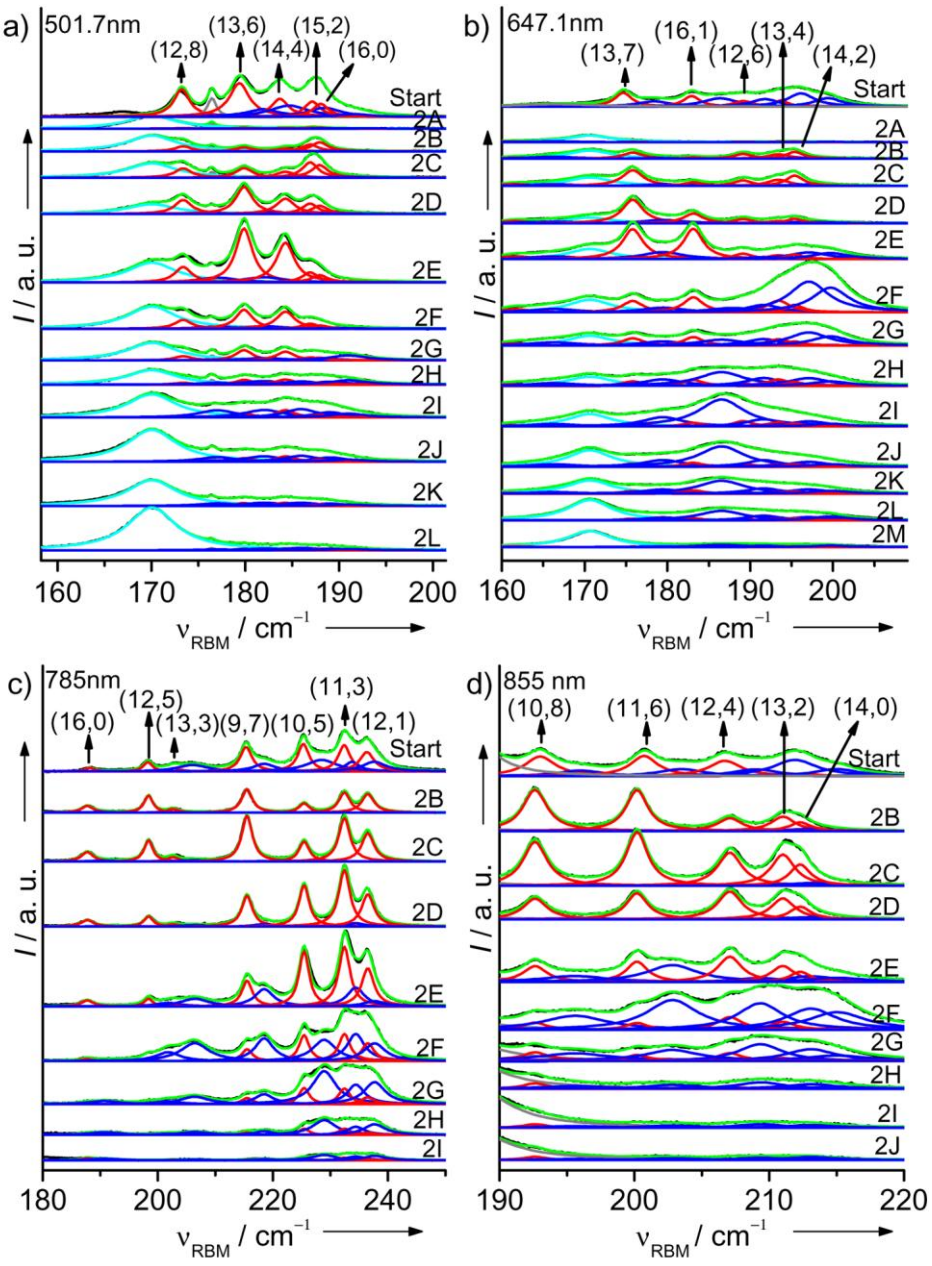

***Figure S6: Resonant Raman spectra and fits of fractions 2A-2M (0.7%w/v SC) excited at different wavelengths*.** RRS spectra (black) are presented together with their best fits (green), composed of two Lorentzians for each SWCNT chirality, corresponding to empty (red) and water-filled (blue) SWCNTs. A Raman band of the gradient medium (cyan), when present, is also implemented in the fit. a) Excitation at 501.7 nm, in the third optical transition of the semiconducting tubes. Also a contribution from a plasma line of the laser (gray) is fitted. b) Excitation at 647.1nm, in the first optical transition of the metallic tubes c) Excitation at 785 nm, in the second optical transition of the semiconducting tubes. d) excitation at 855nm, in the second optical transition of semiconducting tubes. The gray curve in the fit corresponds to tubes further out of resonance. Fractions 2K-2M contain bundles/aggregates, and therefore are not reliably fitted.

Raman spectroscopy, assuming similar cross-sections for empty and water-filled tubes.[2] The present observation that the Raman cross-section of water-filled SWCNTs is in fact significantly reduced, implies that the fractions of water-filled tubes in the experiments of reference [2], and thus the amount of damage occurring in these simple mechanical treatments, is even larger than previously thought.

6. Adapted empirical relations for the SWCNT electronic transition energies

In order to identify the SWCNT peaks observed in the 2D IR fluorescence data (i.e. to plot the peak positions and grids on the 2D IR fluorescence maps; see Figure S8), we used a slightly adapted version of the well-known empirical relations of Bachilo *et al.*[14]. The highly resolved fluorescence-excitation maps which we obtained for purely empty SWCNTs, allowed us to make a very accurate determination of the empirical parameters. These are expected to be slightly different from Bachilo's, because (1) in reference [14] a very different surfactant was used (SDS), and (2) we used empty tubes, whereas in reference [14] mixed (empty and water-filled) samples were used, probably dominated by water-filled tubes (considering the used ultrasonication). For an accurate determination of the new parameters, we determined the best fit to the observed peak positions from both Arc (large diameters, ~1.09 – 1.44 nm) and HipCO (small diameters, ~0.74 – 1.22 nm) sorted empty SWCNTs (for HipCO see Section 10 and Figure S7) to cover a very wide diameter range (0.74 – 1.44 nm). In this way, we obtained the following empirical relations for the first (ν_{11}) and second (ν_{22}) van Hove transition frequencies for a SWCNT (*n*,*m*) as a function of its diameter *d* (in nm, calculated using a carbon-carbon distance of 0.142

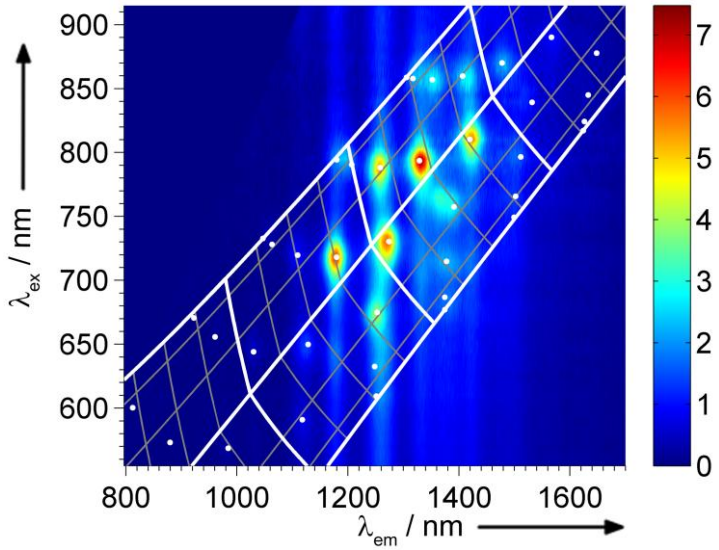

Figure S7: 2D IR fluorescence map of sorted empty HipCO SWCNTs using 2%w/v SC (sample 7). Fluorescence-excitation map of one of the empty SWCNT fractions of the HipCO SWCNTs, which was one of the datasets used (in combination with data for other empty HipCO and Arc SWCNT fractions) to fit the empirical relations (S2) [and (S3)] for the transition energies. The fit values from equations (S2) are superimposed on the experimental data.

nm) and chiral angle α:

$$\nu_{11} = \frac{1\times10^{7}\,\mathrm{cm}^{-1}}{151.4 + 1090.9\,d} + \frac{A_1\cos(3\alpha)}{d^{2}}$$
$$\nu_{22} = \frac{1\times10^{7}\,\mathrm{cm}^{-1}}{145.7 + 581.9 d} + \frac{A_2\cos(3\alpha)}{d^{2}} \qquad \text{(S2)}$$

with $A_1 = -674$ cm^{-1} for (n-m) mod 3=1 ("mod1") and $A_1 = 285$ cm^{-1} for (n-m) mod 3=2 ("mod2") and with $A_2 = 1261$ cm^{-1} for mod1 and $A_2 = -1345$ cm^{-1} for mod2. This yields an excellent fit of the experimental peak positions (see e.g. Figure S7, or any of the other 2D fluorescence maps for empty SWCNTs).

Finally we note that also a more refined form of the original Bachilo relations has been proposed in the literature[15], including eight additional fit parameters (exponents B_i and C_i in the second term). Fitting all parameters in those relations to our experimental data led to:

$$\nu_{11} = \frac{1\times10^{7}\,\mathrm{cm}^{-1}}{131.6 + 1112.2\,d} + \frac{A_1\cos(3\alpha)^{B_1}}{d^{B_2}}$$
$$\nu_{22} = \frac{1\times10^{7}\,\mathrm{cm}^{-1}}{144.2 + 585.6 d} + \frac{A_1\cos(3\alpha)^{C_1}}{d^{C_2}} \qquad \text{(S3)}$$

with $A_1 = -692$ (mod1) or 330 (mod2); A_2=1273 (mod1) or -1396 (mod2); B_1=1.15 (mod1) or 0.96 (mod2); B_2=2.93 (mod1) or 1.87 (mod2); C_1=0.88 (mod1) or 1.12 (mod2) and C_2=1.98 (mod1) or 2.39 (mod2). However, this did not yield a significant further improvement of the fit compared to equations (S2), and therefore we continued to use equations (S2) throughout this work (e.g. to plot the peak positions and to derive the constant density and constant chiral angle grids, see also Section 7).

While the above equations were fitted to data for empty SWCNTs solubilised with 2%w/v SC, no significant deviations were observed when using 0.7% SC. Also, the relations remain useful for empty SWCNTs in the other bile salt surfactant, DOC, resulting in only very slight deviations (both the first and second transition energy typically being red-shifted by ~2-3 meV with DOC, compared to SC). For water-filled SWCNTs, much larger red-shifts occur, varying strongly from one tube chirality to another (see also Section 8).

7. Band-gap fluorescence-excitation maps of sorted DGU fractions and data analysis

In order to facilitate the interpretation of the 2D fluorescence-excitation data, and in particular to monitor the structure sorting of the SWCNTs, we used several visualization and data analysis methods:

Three-color overlays. To compare (up to) three 2D fluorescence-excitation maps, while preserving all information on the individual SWCNT chiralities, we combined them in three-color (red, green, blue; RGB) overlays. To this end, the 2D maps were normalized to their peak value, and then the intensities of each map

were assigned directly to the corresponding color component (R, G, B) of the overlaid image (i.e. the fluorescence intensities are mapped linearly to the color values of the overlay, without changing the origin: black corresponds to zero fluorescence intensity). An example of such an overlay and the corresponding separate 2D fluorescence-excitation maps is shown in Figure S11.

Chirality labels and diameter-chiral angle grids. Peak positions in 2D fluorescence maps (individual ones or overlays) were indicated and labelled with the corresponding SWCNT chiralities (chiral indices (*n*,*m*)) using the empirical relations (S2). In order to allow effects of diameter and chiral angle to be distinguished at a glance, also gridlines of constant diameter *d* and of constant chiral angle α were superimposed on the 2D maps. These were also derived from equations (S2), simply by treating *d* and α as continuous variables. Throughout this work, gridlines were plotted at 0.05 nm diameter steps (bold gridlines every 0.2 nm) and 10° chiral angle steps (see Figure S8).

Projection of 2D fluorescence data to 1D diameter-intensity curves. When one is only interested in the diameter of SWCNTs in a sample, absorption spectra have the advantage of giving a quick overview, but the wavelength axis cannot be related directly to diameter alone, as transition wavelengths also depend on chiral angle. Fluorescence-excitation data on the other hand allows one to disentangle both diameter and chiral angle information, but its 2D nature at the same time makes it more difficult to comprehend at a glance. It is however possible to combine the advantages of both, by projecting the 2D fluorescence-excitation data along curves of constant diameter, yielding a curve of intensity as a function of the diameter of the contributing SWCNTs (with a resolution only limited by the linewidth of the transitions). This is achieved by integrating the intensity of the 2D map over strips corresponding to narrow diameter intervals [*d*, *d*+δ*d*]. These strips are extended beyond the theoretical limits marked by α = 30°, to avoid truncating intensity that can be present outside this theoretical range due to the finite linewidth of the transitions. To this end, the aforementioned curves of constant diameter were rewritten as a direct relation between λ_{11} (=1/ν_{11}) and λ_{22} (=1/ν_{22}), by eliminating α (and (*n*–*m*) mod 3) from equations (S2), which gives

$$\lambda_{11}(d,\lambda_{22}) = \max\left\{\frac{1261}{(285771.3+1469042.5\,d)/D - 674/\lambda_{22}}, \frac{1345}{(47823.1+218712.4\,d)/D - 285/\lambda_{22}}\right\} \qquad \text{(S4)}$$
$$\textit{with} \quad D = (151.4+1090.9\,d)(145.7+581.9\,d)$$

and where taking the maximum of the two expressions ensures that the correct value of (*n*-*m*) mod 3 is selected for the given combination of *d* and λ_{22}. Equation (S4) thus yields a convenient expression to calculate the needed integration boundaries for each excitation wavelength λ_{22}, which has the important advantage that (S4) can be used to extrapolate the constant diameter curves sufficiently beyond (but not infinitely beyond) the theoretically allowed range of α < 30°.

Thus, this procedure allows us to extract the 1D diameter dependent information from the 2D fluorescence data, through a straightforward integration (i.e. without involving any peak fitting).

Additional 2D fluorescence maps. The 2D IR fluorescence maps of the different fractions of sample 1-3 are given in Figures S9-S11. These were used to produce the overlays given in the manuscript (Figures 2 and 5).

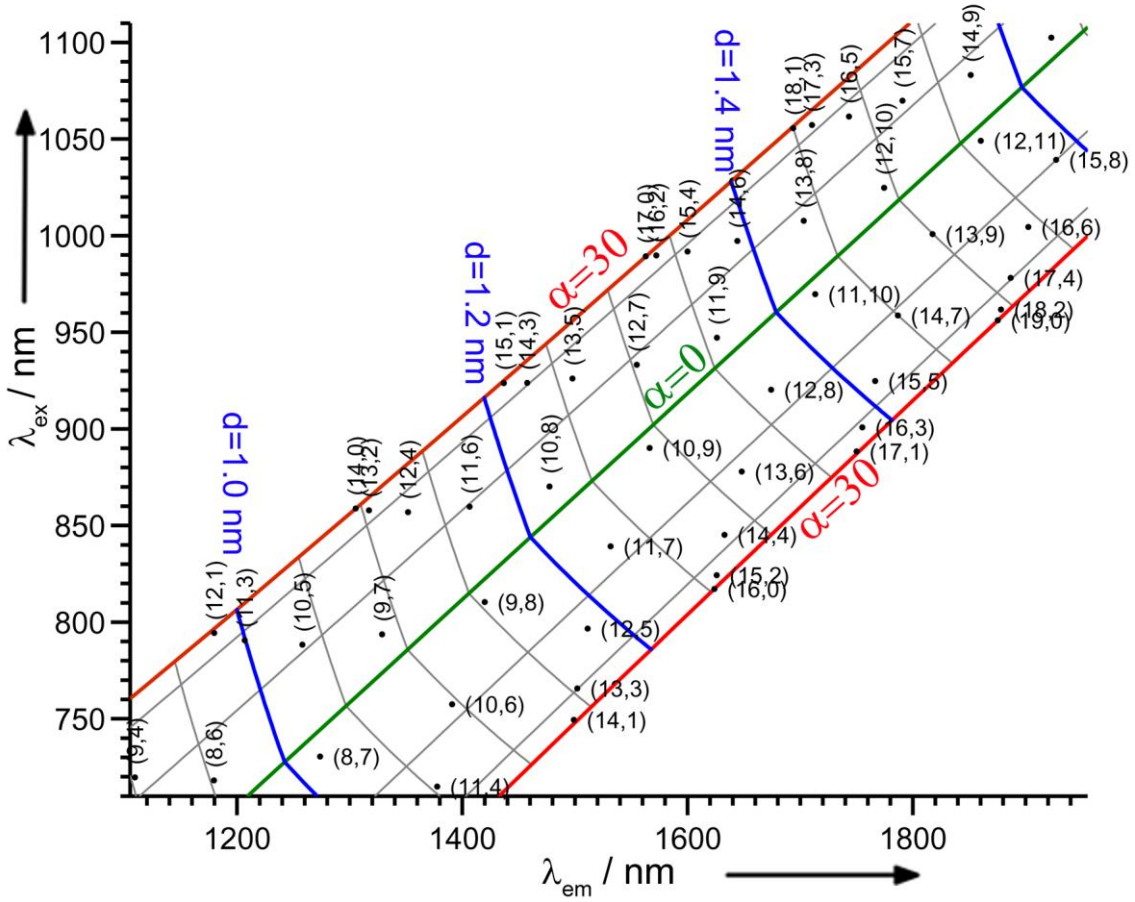

***Figure S8: Peak positions of the SWCNTs in the 2D IR fluorescence-excitation maps*.** Peak positions were determined by adapting the well-known Bachilo empirical relations[20] to fit our experimental data for empty SWCNTs (see Section 6, equations (S2)). The constant diameter – constant chiral angle grid is based on the same relations. As in all such grids on 2D fluorescence maps throughout this paper, diameter gridlines are drawn at 0.05 nm intervals, with bold lines (here in blue) at 0.2 nm intervals, and chiral angle gridlines are drawn at 10˚ intervals with bold lines at 0˚ (here in green; tubes near this line have a close to armchair geometry) and 30˚ (here in red; zigzag tubes). SWCNTs with ($n - m$) mod 3 = 1 are found in the region to the lower right of the green $\alpha = 0^\circ$ line, SWCNTs with ($n - m$) mod 3 = 2 to the upper left of it.

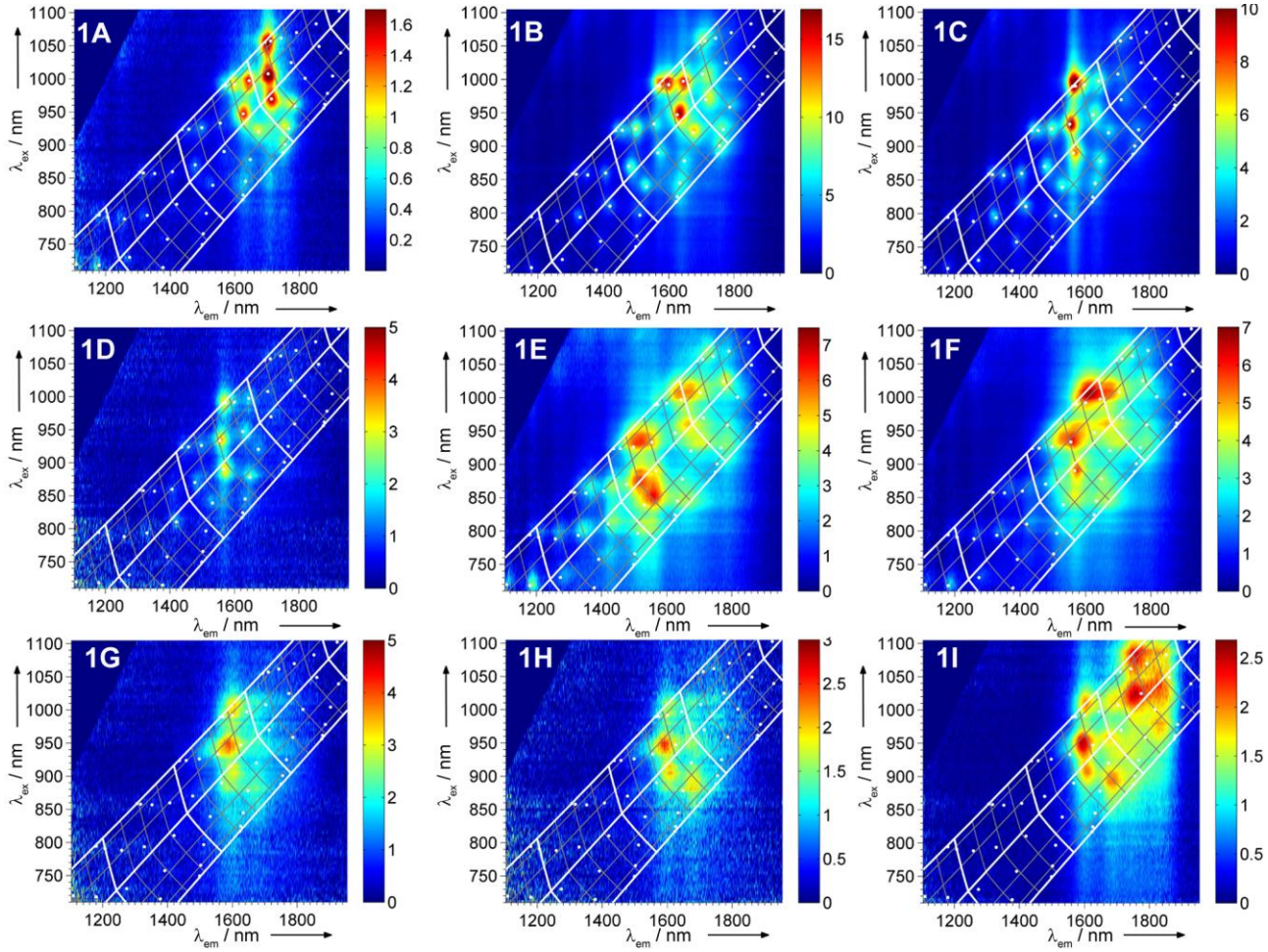

Figure S9: 2D IR fluorescence maps of sample 1 (2%w/v SC). Fluorescence spectra of all fractions of sample 1 (see Figure 1 in the main text), clearly showing the inverse diameter sorting for empty (fractions 1A-1D) and water-filled (fractions 1E-1I) tubes. White dots are predicted SWCNT positions using the adapted empirical relations for empty tubes (see Section 6), and gridlines indicate diameter and chiral angle as in Figure S8. From this the electronic shifts of both the first and second van Hove transition upon water-filling can be clearly observed. Average densities of fractions 1A- 1I are, respectively, 1.163, 1.175, 1.182, 1.192, 1.199, 1.204, 1.218, 1.229, and 1.267 g mL^{-1}.

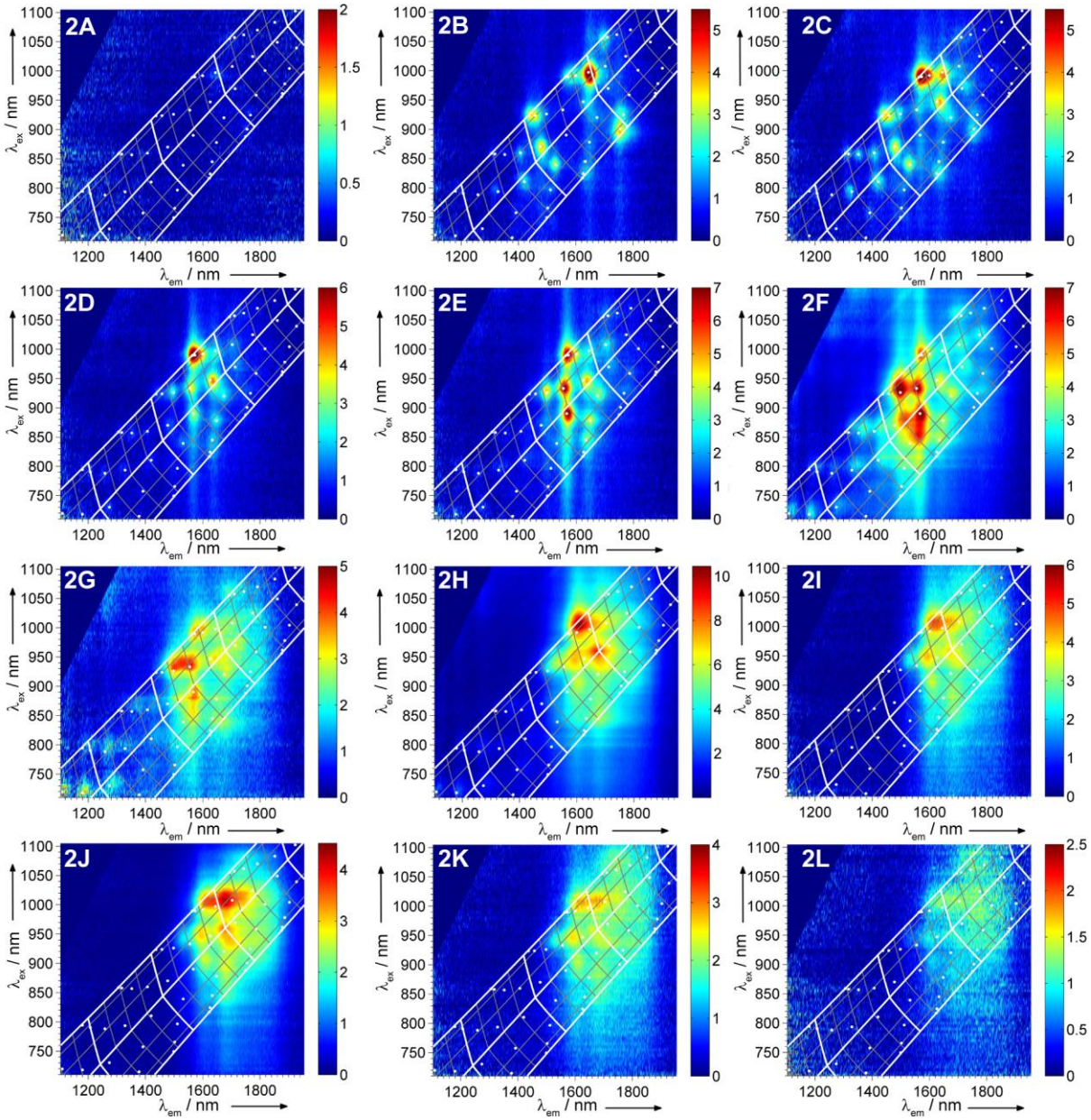

Figure S10: 2D IR fluorescence maps of sample 2 (0.7%w/v SC). Fluorescence spectra of all fractions of sample 2 (see Figure 4a in the main text), clearly showing the diameter sorting of the SWCNTs, with a reversal occurring at a diameter of ~1.3nm for the empty tubes, ascribed to surfactant effects. White dots are predicted SWCNT positions using the adapted empirical relations (see Section 6), and gridlines indicate diameter and chiral angle as in Figure S8. Average densities of fractions 2A-2L are, respectively: 1.160, 1.168, 1.171, 1.187, 1.190, 1.211, 1.222, 1.232, 1.253, 1.258, 1.264, and 1.293 g mL^{-1}.

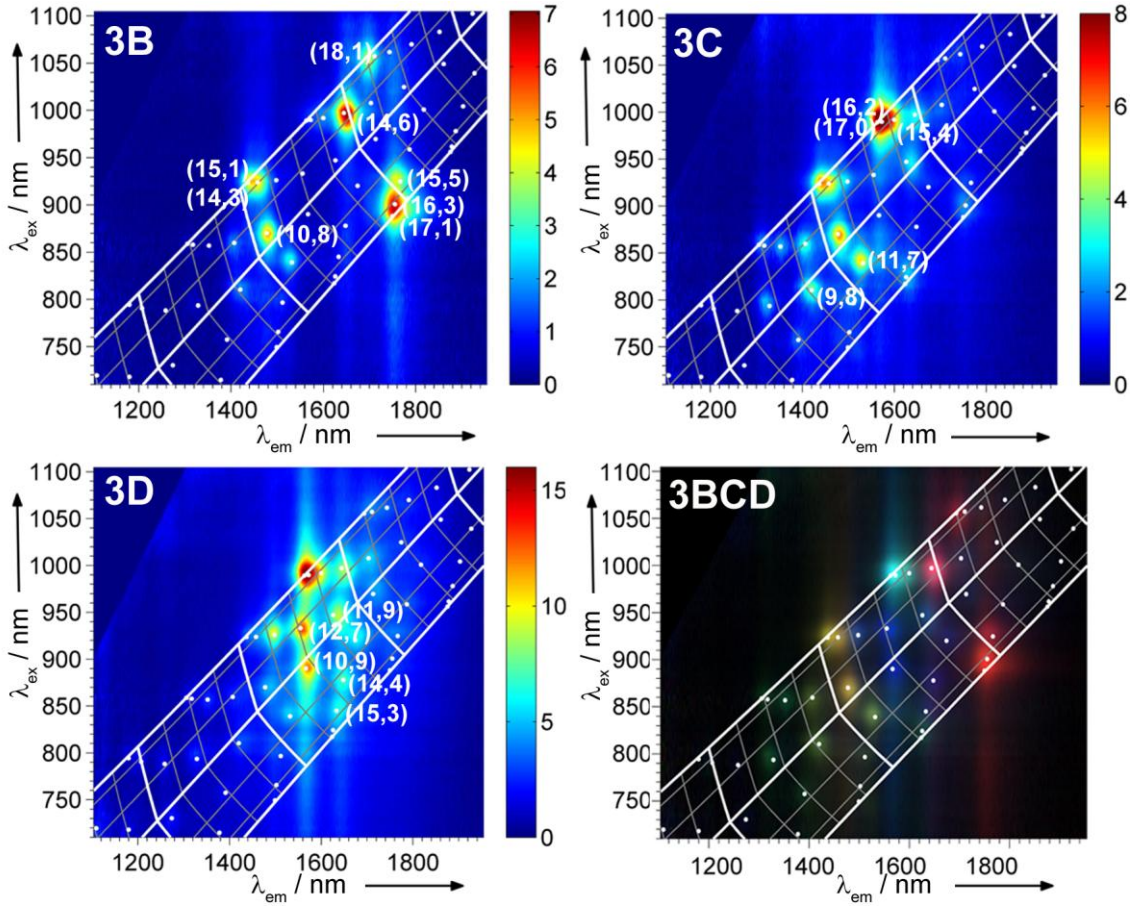

Figure S11: 2D IR fluorescence maps of sample 3 (0.7%w/v SC). Fluorescence spectra of the empty fractions of sample 3 (see Figure 4c in the main text), clearly showing the diameter sorting of the SWCNTs with a reversal occuring at a diameter of ~1.3 nm for the empty tubes, ascribed to surfactant effects. The fluorescence in combination with the absorption spectra (Figure 4d) show a very good sorting with only a few chiralities dominating in each fraction. White dots are predicted SWCNT positions using the adapted empirical relations (see Section 6), and gridlines indicate diameter and chiral angle as in Figure S8. The lower right panel shows a three-colour overlay of the fluorescence spectra of fractions 3B (red), 3C (green) and 3D (blue), where the individual spectra were normalized. Average densities of fractions 3B-3D are, respectively: 1.176, 1.194 and 1.204 g mL^{-1}.

8. Relative fluorescence quantum efficiency of empty and water-filled SWCNTs

By comparing the 2D IR fluorescence maps of the empty and filled fractions (see Section 7) with the optical density of the samples, we found that the empty SWCNTs have considerably higher fluorescence quantum efficiencies than the water-filled SWCNTs. Care was taken to keep the absorbance of the solutions sufficiently low, to allow for an accurate correction for reabsorption when quantifying the relative quantum efficiencies. In Figure S12 the 1D fluorescence spectra excited at three different wavelengths are given for a sample which was separated in only two fractions (empty and water-filled tubes, respectively; see also Figure S4 for the absorption spectra of these two fractions). In Figure S12, the fluorescence intensities were normalized to the optical density of the SWCNT van Hove transitions, at the corresponding excitation wavelength. First of all note that once

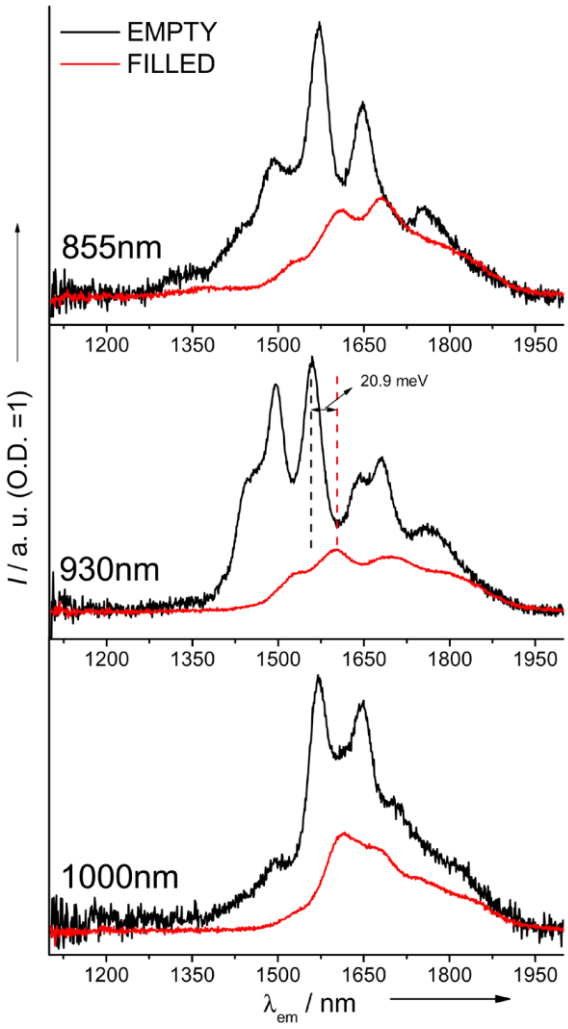

Figure *S12: Quantum efficiency of empty and water-filled SWCNTs.* 1D Fluorescence spectra of samples containing only empty and only water-filled SWCNTs excited at different wavelengths. Fluorescence intensities are normalized to the optical density of the fractions at the respective excitation wavelengths. Empty tubes have narrower line widths and higher fluorescence quantum efficiencies than water-filled tubes. Specifically for these excitation wavelengths, the empty SWCNTs have a factor of 1.78 (855 nm), 2.45 (930 nm), and 2.05 (1000nm) higher quantum efficiencies. Electronic shifts of the resonances are also very clearly observed.

again, the electronic red-shifts upon water-filling are very clear. Secondly, it can be observed that the empty SWCNTs have narrower resonance lines than the water-filled tubes. Finally, by comparing the integrated intensities, we found the band-gap fluorescence quantum efficiency (QE) to be (more than) twice as high for the empty SWCNTs than for the water-filled ones (QE(empty)/QE(water-filled) = 1.78, 2.45, and 2.05 for SWCNTs excited at 855 nm, 930 nm, and 1000 nm, respectively).

Besides the difference in quantum efficiency for empty and water-filled SWCNTs, the quantum efficiency also depends on the diameter of the SWCNTs.[16] This diameter dependence is very strong in the range of large diameters considered in this work. This is very clear after integration of the 2D fluorescence spectra over all excitation wavelengths or over all emission wavelengths and plotting this on the absorption spectra of, respectively, the second or first transition of the same fractions (see Figure S13). Figure S13 clearly shows that

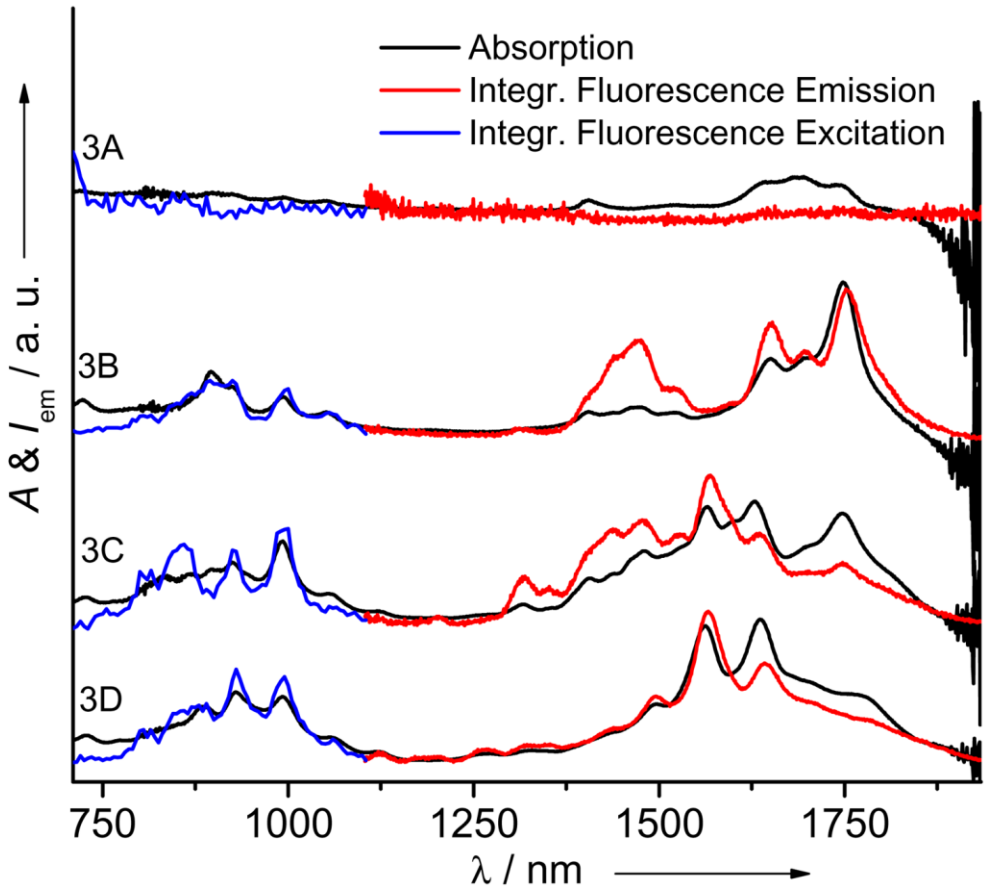

Figure S13: Quantum efficiency dependence on diameter. Absorption (black) and integrated fluorescence emission/excitation (red/blue) spectra for fractions 3A-3D. Excitation spectra (blue; plotted in the second electronic transition region, from 710-1110nm) are integrated over all emission wavelengths. Emission spectra (red; plotted in the first transition region, from 1110-1950nm) are integrated over all excitation wavelengths. The comparison of absorption and fluorescence spectra reveals a strong diameter dependence of the fluorescence quantum efficiency (QE) with higher QE for thinner SWCNTs. Note that the resolved features in the emission spectra (first optical transition region) show small Stokes-shifts with respect to the absorption resonances.

the fluorescence quantum efficiency drastically drops for larger diameter SWCNTs: compared with absorption spectra, in fluorescence spectra the shorter wavelength peaks are strongly enhanced relative to the longer wavelength peaks. It is important to take this into account when using fluorescence-excitation spectroscopy to quantify the composition of SWCNT samples. For instance, this also implies that the very narrow chirality distributions of large diameter tubes found from the fluorescence spectra of the upper fractions of sample 3 (e.g. fraction 3B in Figure 5a in the main text), are in fact even narrower taking into account that the small amount of thinner tubes still present is overrepresented in the fluorescence spectra (e.g. comparison with the absorption spectrum of 3B, in Figure 4, indeed shows that this fraction is dominated by the thick (17,1)/(16,3) SWCNTs). Conversely, the purity of small diameter tubes may be overestimated when relying on fluorescence data only, as contamination with larger diameter tubes will be less apparent.

The red-shifts of the electronic transitions upon water-filling can be determined most accurately from the 2D fluorescence excitation maps of the DGU sorted fractions (e.g. Figures S9, S10 & S12, and Figure 2d in the main text) which show the transitions of individual SWCNT chiralities and their water-filled counterparts. We found red-shifts of 10 meV on average (both for the first and second electronic transition), with typical values in the range of 4–20 meV (depending on tube chirality), in line with the red-shifts observed also in the absorption spectra (see Section 3 and Figures S3-S4).

9. DGU sorting with 2% w/v DOC (Arc SWCNTs)

Besides sodium cholate (SC), we also explored the possibilities of using sodium deoxycholate (DOC) in the DGU sorting experiments. DOC was previously found to be a better surfactant to solubilise SWCNTs,[1, 17] but it is less popular in DGU work, because it yields a much lower selectivity in the DGU sorting of small diameter SWCNTs.[18] Figure S14 shows the image of the centrifuge tube, absorption and RRS and fluorescence spectra of a DGU sorted sample of Arc SWCNTs with 2%w/v DOC. Here too, the same general trends are observed

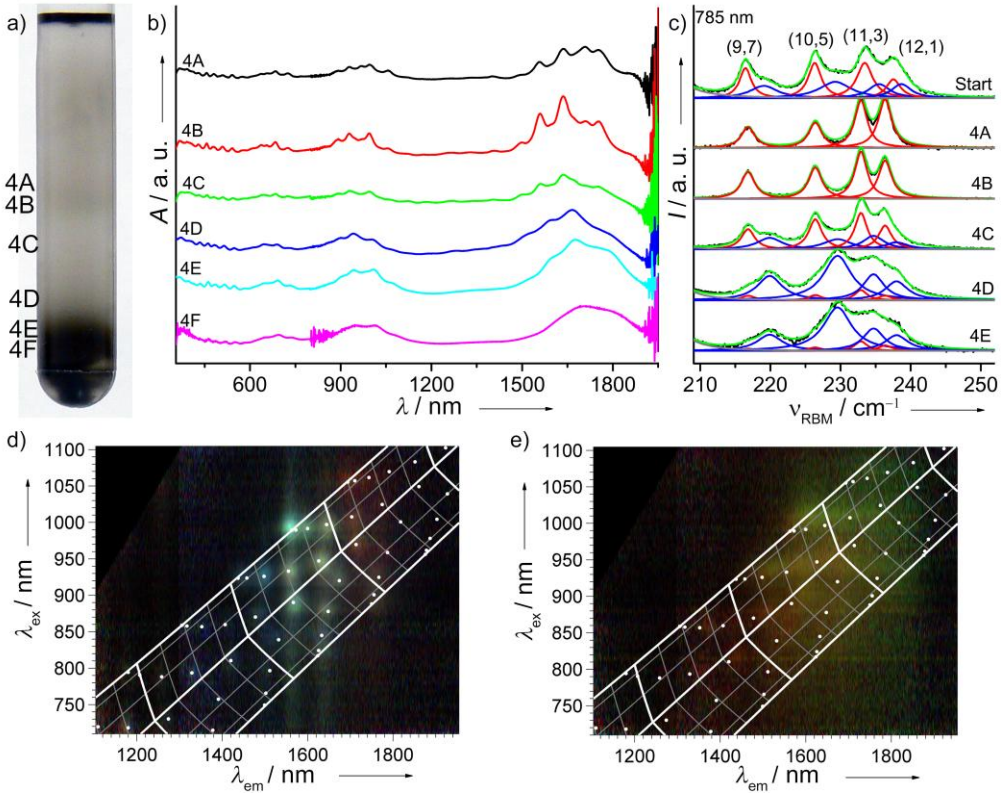

Figure S14: Sorting of Arc SWCNT solutions with 2%w/v DOC. a) Image of the centrifuge tube. b) Absorption spectra of the different fractions c) RRS excited at 785 nm, clearly showing the RBM resonances of empty (red) and water-filled (blue) SWCNTs. d) Three-colour overlay of the fluorescence data of fractions 4A (red), 4B (green) and 4C (blue). e) Three-colour overlay of the fluorescence data of fractions 4D (red), 4E (green) and 4F (blue). Average densities of fractions 4A-4F are, respectively: 1.164, 1.180, 1.185, 1.199, 1.22, and 1.23 g mL^{-1}.

with an inverse sorting for empty and water-filled SWCNTs, and narrower spectral line widths for empty tubes compared to water-filled tubes. However, the general trend of density vs. diameter is more systematic (e.g. Figure S14d shows a monotonous dependence), with much less oscillations, further supporting the idea that these oscillations are related to surfactant layer packing effects. This smoother, more systematic diameter-density relation (in good agreement with the trend predicted by the simple geometric model of Section 2) is also confirmed for smaller diameter SWCNTs, even when using only 0.7%w/v DOC, by experiments with HipCO SWCNTs (see Section 10; Figures S19-S20).

10. Separation of empty and water-filled HipCO SWCNTs, with SC *vs*. DOC

Also for the HipCO SWCNTs, which have a much broader diameter distribution, the empty tubes could be separated from the filled tubes. Using DOC as a surfactant (see Figure S18), both thinner diameter ($d \approx 0.458$ nm) and thicker diameter ($d \approx 1$ nm) empty tubes could be isolated. When using SC as a surfactant, the absorption spectra indicate a more selective (yet less systematic) *diameter* sorting than for DOC, however, the Raman spectra reveal that empty and filled tubes are not separated as well (see Figure S16), in particular for the thinnest SWCNTs. This indicates that with SC, the surfactant packing effects (which probably dominate the diameter sorting for small diameter tubes[4b]) causes large amplitude oscillations in the diameter-density relation, which interfere with the systematic diameter-density dependence and with the separation of empty and water-filled tubes. This is confirmed by the observed diameter-density relations for SWCNTs solubilised with SC (Figure S18: large oscillations), compared to DOC (Figure S20: much smoother dependence). The surfactant-induced oscillations are also significantly more pronounced at lower surfactant concentration (0.7%w/v SC; Figure S18), than at high surfactant concentration (2%w/v SC; Figure 3 in the main text), in good agreement with the recent observations by Ghosh *et al*. of excellent DGU sorting of small diameter SWCNTs at this lower SC concentration.[5] It is indeed not unlogical that the surfactant coating becomes most SWCNT structure dependent as the surfactant concentration is decreased, eventually approaching the critical concentration for forming an adsorbed micellar coating (in fact, at 0.7%w/v, a partial reaggregation of the SWCNTs is observed during centrifugation, while at 2%w/v, very stable solutions are formed, without any sign of reaggregation; e.g. compare Figures 1a and 4a, where the lower surfactant concentration results in the presence of bundles after DGU, even though both DGU runs were started from the same SWCNT solution).

Note that the only difference between SC and DOC is that the cholesterol group of SC bears three OH groups, all on the same side of the cholestorol group, whereas DOC has only two (see Figure S15). The effects of this may be twofold: (1) The higher polarity of SC makes it more water-soluble, and therefore increases its critical micelle concentration.[19] (2) The three OH groups of SC divide the flattened bean shape of the cholesterol group into a polar and an apolar face,[19] so that when adsorbed on a SWCNT, it is very likely to adsorb with its apolar face flat onto the SWCNT – thus creating a 2D stacking which may or may not fit well with the circumference of the tube. In DOC on the other hand, the two OH groups create only one polar edge, which may result in other orientations on the SWCNT surface, possibly tilted and partially overlapping, which would allow for a more flexible and gradual adaptation to different SWCNT diameters (see Figure S15), explaining the absence of pronounced oscillations in the density-diameter relation for DOC.

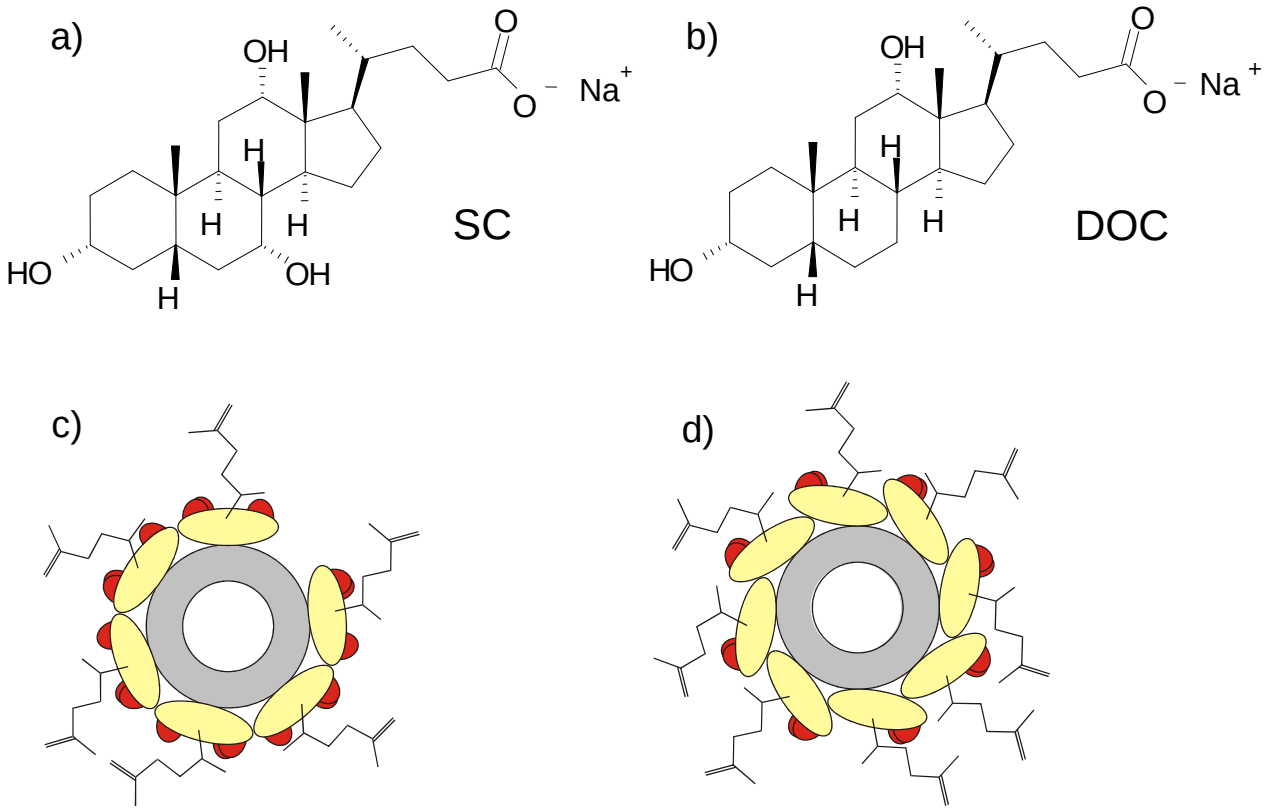

Figure S15: Chemical structure of SC and DOC and possible differences in their packing. a)-b) The chemical structures of sodium cholate (SC, a) and sodium deoxycholate (DOC, b). c)-d) Schematic representation of a possible difference in the ordering of SC (c) and DOC (d) surfactants around a SWCNT (gray): the presence of only two polar OH groups (red) on the semi-rigid cholesterol group (yellow) of DOC may allow for more overlap of neighbouring surfactant molecules and for a more flexible adaptation of the packing to different nanotube diameters.

The structure of the surfactant packing around the SWCNTs for these and other bile salts certainly deserves further study. In any case, it is clear that the surfactant-induced density variations (which are enhanced by using a low surfactant concentration) can play a dominant role in the diameter sorting of small diameter tubes, while at large diameters, the general trend of decreasing density with increasing diameter for empty SWCNTs becomes more important, and may be either enhanced or counteracted by surfactant effects. These surfactant effects can be reduced by using higher surfactant concentrations and/or a surfactant which yields a more uniform diameter-independent coating such as DOC. The latter is desirable for isolating empty SWCNTs. Note that the present results show that the higher selectivity obtained with SC is due to the more critical diameter-sensitivity of the SC coating, rather than its higher homogeneity,[18] which solves the long-standing apparent contradiction of SC providing better diameter sorting,[4b] despite DOC being a more effective surfactant in terms of achievable SWCNT concentrations, and both providing very homogeneous coatings as judged from the extraordinarily narrow spectral line widths.[1, 17]

Besides DOC being a more effective surfactant for solubilising SWCNTs in general,[1, 17] we now also found that DOC is in particular a much better surfactant for the thinnest tubes: e.g. the (5,3) SWCNTs, the very thinnest tubes observed, could only be found in DOC solubilised samples. Also note that these results for the

thinner HipCO SWCNTs nicely illustrate that once the empty SWCNTs are isolated, extraordinarily well-resolved Raman spectra are obtained (see e.g. fractions 6B and 6C in Figure S18d-e; e.g. RBM linewidth of 1.16 cm^{-1} for the (6,5) tube).

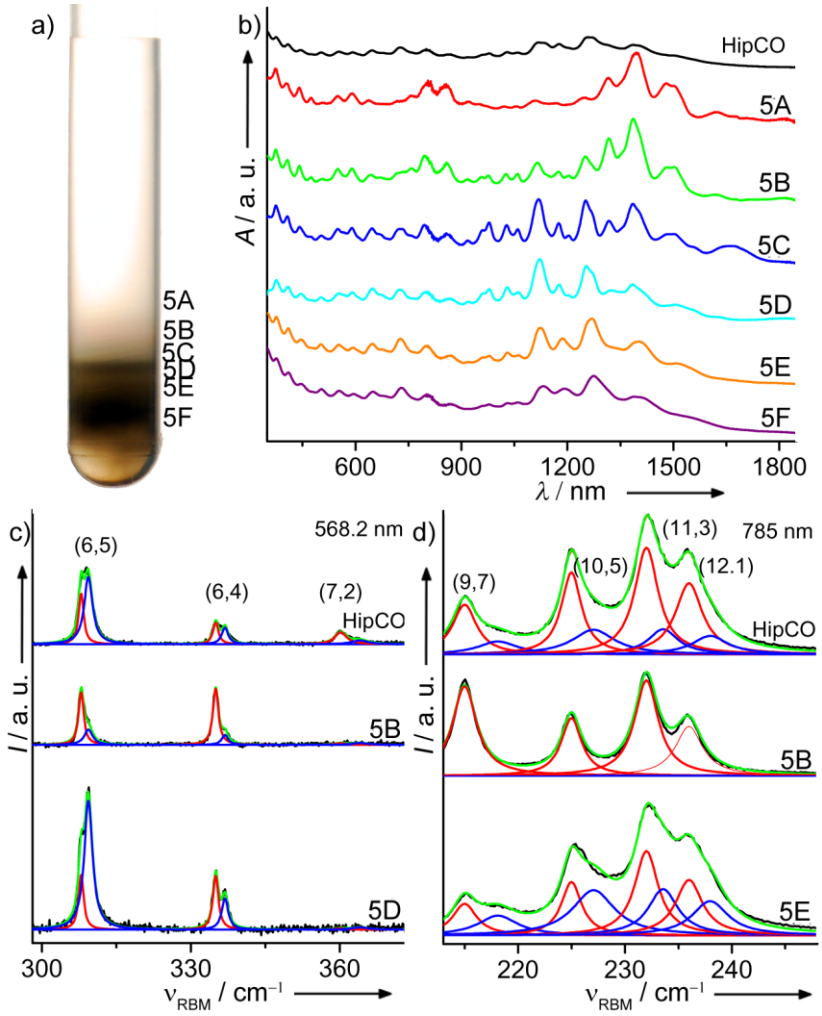

Figure S16: Separation of empty and water-filled HipCO SWCNTs using 0.7%w/v SC. a) Photograph of the centrifuge tube b) Optical absorption spectra of unsorted HipCO sample and of the sorted fractions. c) and d): RRS spectra (black) excited at 568.2 nm (c) and at 785nm (d) together with their best fits (green), composed of two Lorentzians for each SWCNT chirality, corresponding to empty (red) and water-filled (blue) SWCNTs. Average densities of fractions 5A-5E are, respectively: 1.171, 1.183, 1.185, 1.213, 1.230, and 1.286 g mL^{-1}.

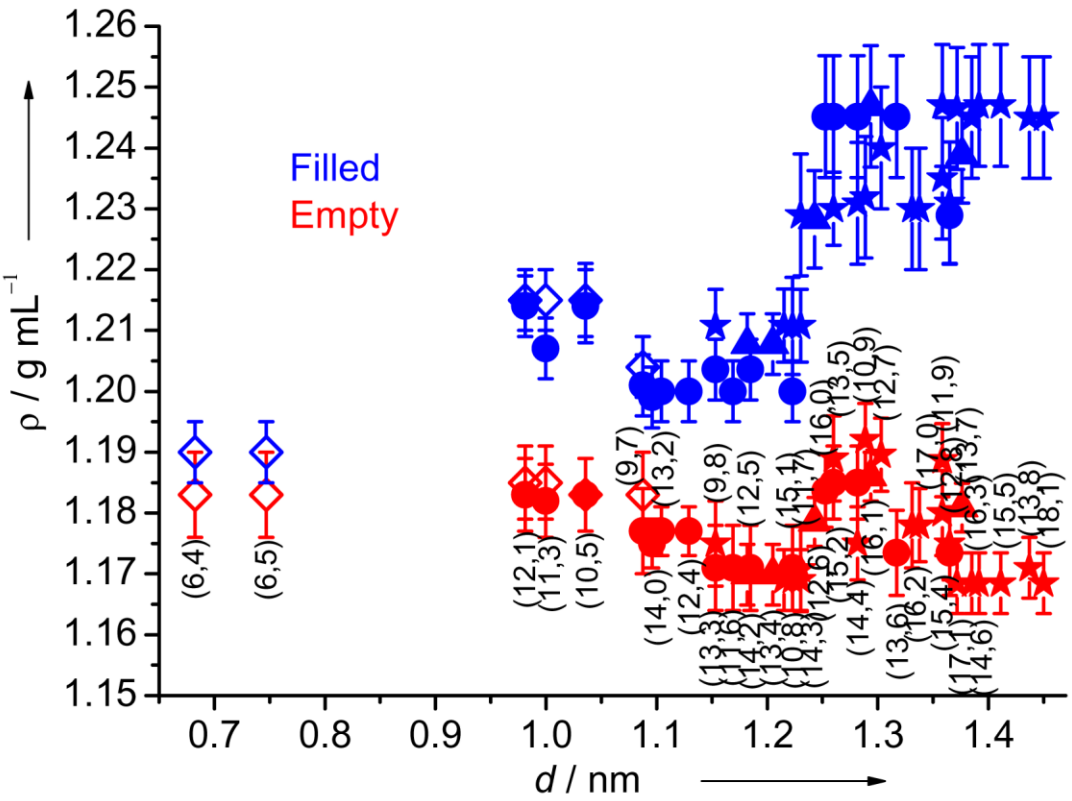

Figure S17: Density of empty and water-filled SWCNTs using 0.7%w/v SC. Plot of the buoyant density of empty (red) and water-filled (blue) SWCNTs in 0.7%w/v SC, as in Figure 5b in the main text, but extended with Raman based data for smaller diameters from HipCO SWCNT sample 5 (open diamonds).

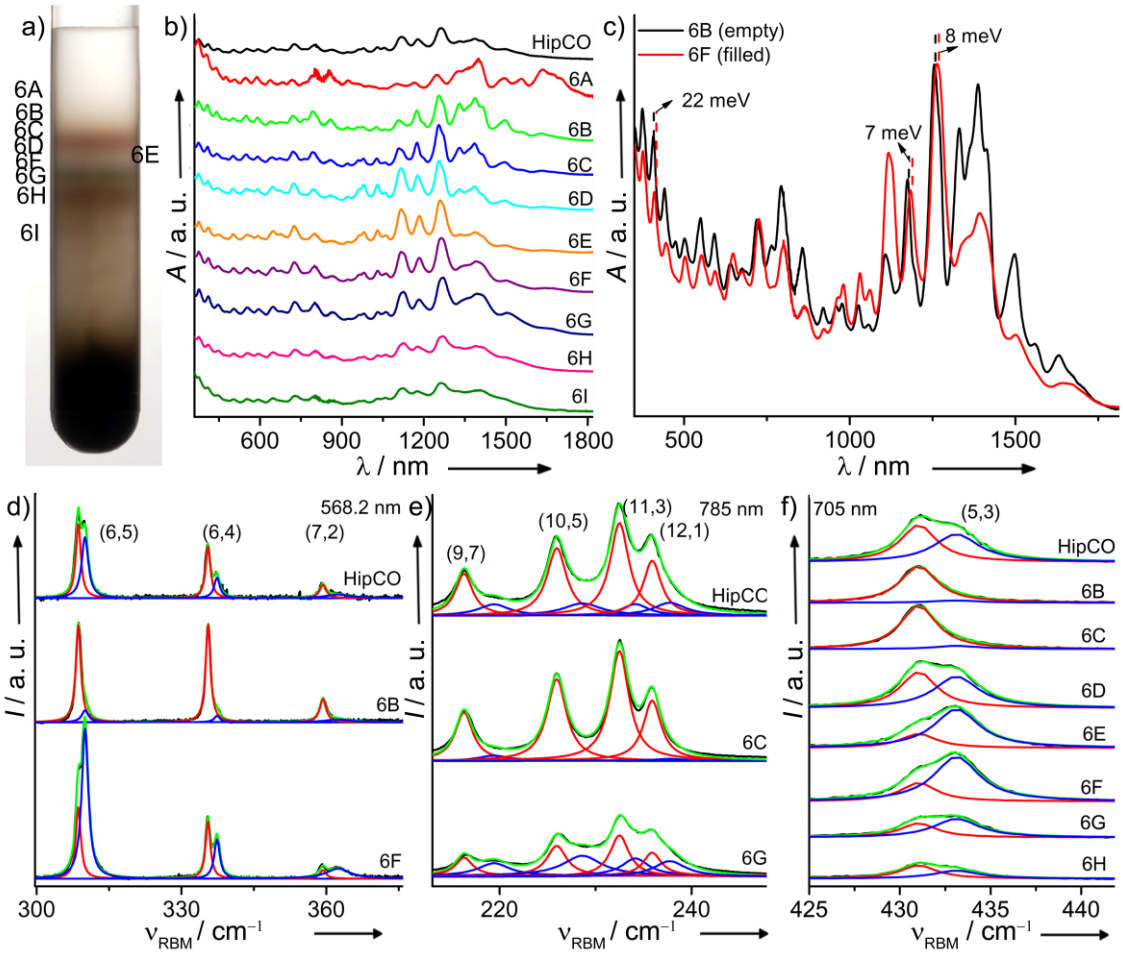

***Figure S18: Sorting of empty and water-filled HipCO SWCNTs using 0.7%w/v DOC*.** a) Photograph of the centrifuge tube b) Optical absorption spectra of unsorted HipCO sample and of the sorted fractions; c) Comparison of the absorption spectrum of empty and filled SWCNT fractions, clearly showing the red-shifts due to water-filling. d)-f): RRS spectra (black) excited at 568.2 nm (d), 785 nm (e), and 705 nm (f) together with their best fits (green), composed of two Lorentzians for each SWCNT chirality, corresponding to empty (red) and water-filled (blue) SWCNTs. The RRS spectra excited at 705 nm are in resonance with the (5,3) tubes, the thinnest SWCNTs observed. Note that in all cases an excellent isolation of the empty species was achieved. Average densities of fractions 6A-6I are, respectively: 1.154, 1.176, 1.179, 1.183, 1.207, 1.211, 1.220, 1.267, and 1.375 g mL^{-1}.

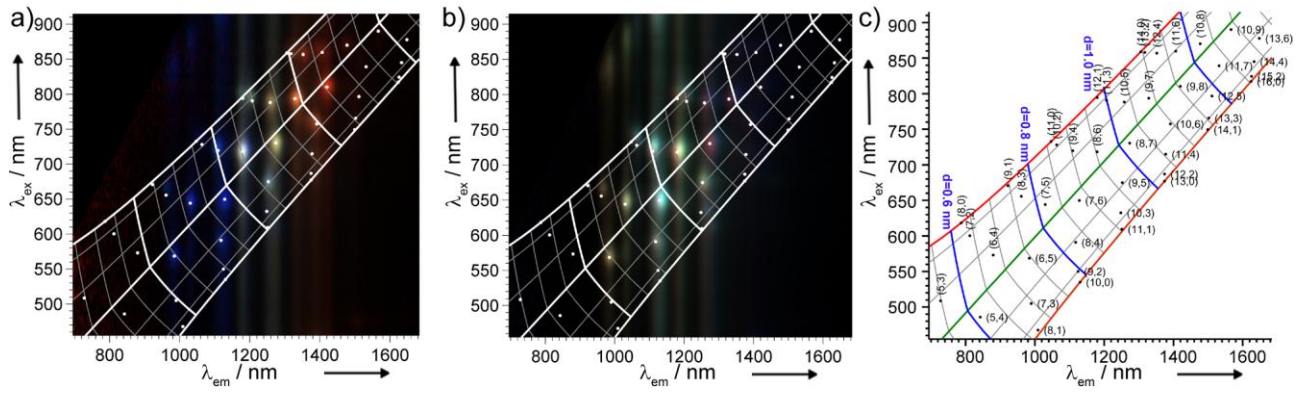

Figure S19: Fluorescence of sorted HipCO SWCNTs with 0.7%w/v DOC. a) overlay plot of fractions 6B (red), 6C (green) and 6D (blue), representing mainly empty SWCNTs. b) Overlay plot of fractions 6D (red), 6F (green), 6G (blue), with 6F and 6G containing mainly filled SWCNTs. c) predicted peak positions for the HipCO SWCNTs according to the adapted empirical relations [equations (S2)].

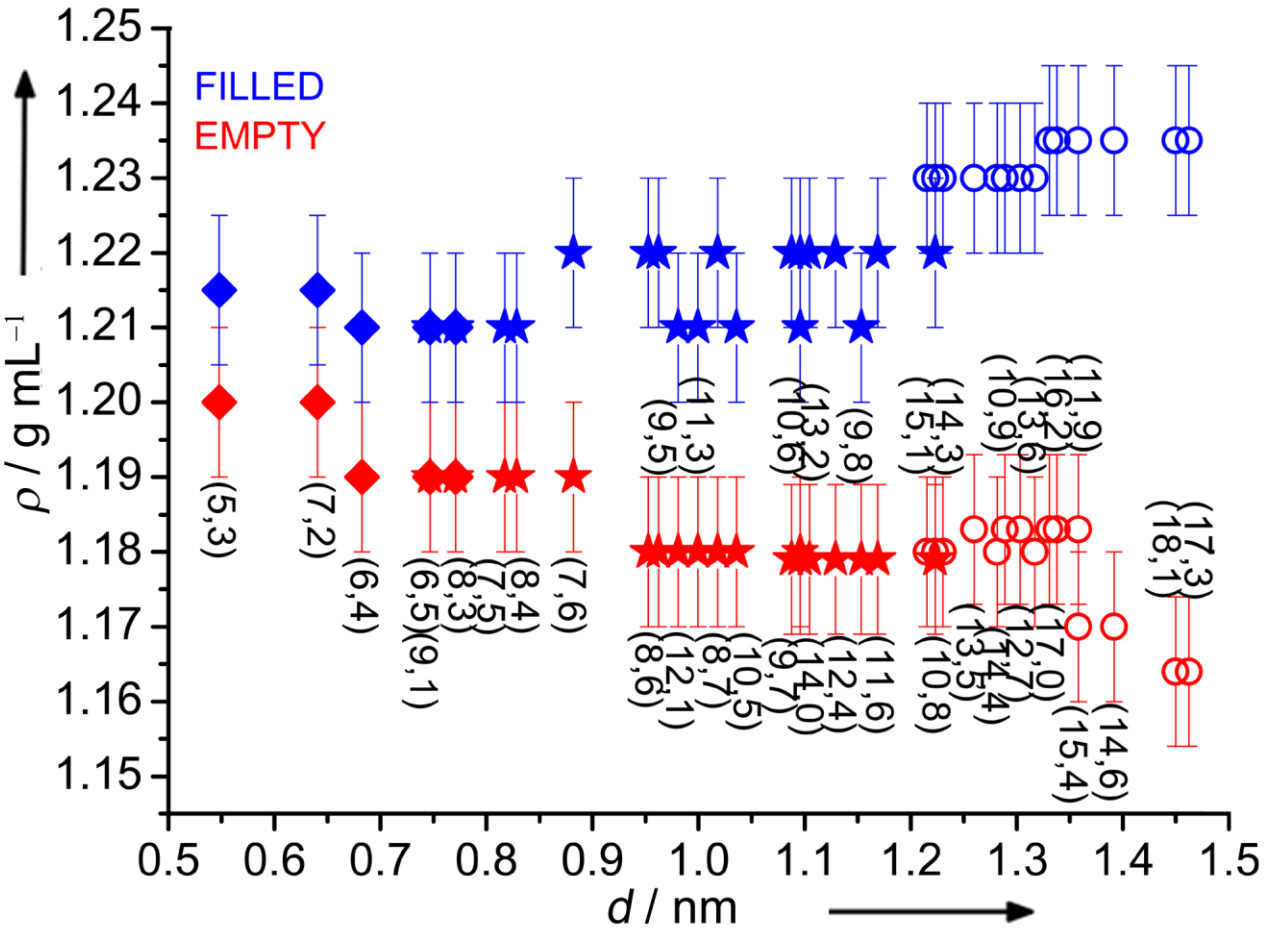

Figure S20: Diameter-density relation for SWCNTs with DOC. Plot of the buoyant density of empty (red) and water-filled (blue) SWCNTs, as in Figure 3 in the main text, but using DOC as surfactant. Filled symbols: HipCO SWCNTs with 0.7%w/v DOC (sample 6); open symbols: Arc SWCNTs with 2%w/v DOC (sample 4); diamonds: data derived from Raman spectrometry; stars are based on fluorescence data. This shows that a more systematic, monotonous dependence on diameter is observed when using DOC as surfactant.

References:

[1] W. Wenseleers, I. I. Vlasov, E. Goovaerts, E. D. Obraztsova, A. S. Lobach, A. Bouwen, *Adv. Funct. Mater.* **2004**, *14*, 1105.

[2] W. Wenseleers, S. Cambré, J. Culin, A. Bouwen, E. Goovaerts, *Adv. Mater.* **2007**, *19*, 2274.

[3] D. Rickwood, T. Ford, J. Graham, *Anal. Biochem.* **1982**, *123*, 23.

[4] a) N. Nair, W. J. Kim, R. D. Braatz, M. S. Strano, *Langmuir* **2008**, *24*, 1790; b) M. S. Arnold, A. A. Green, J. F. Hulvat, S. I. Stupp, M. C. Hersam, *Nature Nanotechnol.* **2006**, *1*, 60; c) J. A. Fagan, M. L. Becker, J. H. Chun, P. T. Nie, B. J. Bauer, J. R. Simpson, A. Hight-Walker, E. K. Hobbie, *Langmuir* **2008**, *24*, 13880; d)C. A. Price, *Centrifugation in Density Gradients*, Academic Press, Inc., New York, **1982**.

[5] S. Ghosh, S. M. Bachilo, R. B. Weisman, *Nature Nanotechnol.* **2010**, *5*, 443.

[6] M. Tanaka, S. Kaneshina, K. Shin-no, T. Okajima, T. Tomida, *J. Coloid. Interface Sci.* **1974**, *46*, 132.

[7] R. C. Haddon, J. Sippel, A. G. Rinzler, F. Papadimitrakopoulos, *MRS Bulletin* **2004**, *29*, 252.

[8] S. Cambré, B. Schoeters, S. Luyckx, E. Goovaerts, W. Wenseleers, *Phys. Rev. Lett.* **2010**, *104*, 207401.

[9] A. Quintilla, F. Hennrich, S. Lebedkin, M. M. Kappes, W. Wenzel, *Phys. Chem. Chem. Phys.* **2010**, *12*, 902.

[10] a) M. S. Arnold, J. Suntivich, S. I. Stupp, M. C. Hersam, *ACS Nano* **2008**, *2*, 2291; b) E. J. F. Carvalho, M. C. dos Santos, *ACS Nano* **2010**, *4*, 765; c) C. Backes, E. Karabudak , C. D. Schmidt, F. Hauke, A. Hirsch, W. Wohlleben, *Chem. Eur. J.* **2010**, DOI: 10.1002/chem.200903461

[11] G. T. Pickett, M. Gross, H. Okuyama, *Phys. Rev. Lett.* **2000**, *85*, 3652.

[12] a) K. Koga, G. T. Gao, H. Tanaka, X. C. Zeng, *Nature* **2001**, *412*, 802; b) A. Alexiadis, S. Kassinos, *Chem. Rev.* **2008**, *108*, 5014.

[13] a) R. Fleurier, J. S. Lauret, U. Lopez, A. Loiseau, *Adv. Funct. Mater.* **2009**, *19*, 2219; b) J. Liu, M. C. Hersam, *MRS Bulletin* **2010**, *35*, 315.

[14] S. M. Bachilo, M. S. Strano, C. Kittrell, R. H. Hauge, R. E. Smalley, R. B. Weisman, *Science* **2002**, *298*, 2361.

[15] R. B. Weisman, S. M. Bachilo, *Nano Lett.* **2003**, *3*, 1235.

[16] D. A. Tsyboulski, J.-D. R. Rocha, S. M. Bachilo, L. Cognet, R. B. Weisman, *Nano Lett.* **2007**, *7*, 3080.

[17] R. Haggenmueller, S. S. Rahatekar, J. A. Fagan, J. H. Chun, M. L. Becker, R. R. Naik, T. Krauss, L. Carlson, J. F. Kadla, P. C. Trulove, D. F. Fox, H. C. DeLong, Z. C. Fang, S. O. Kelley, J. W. Gilman, *Langmuir* **2008**, *24*, 5070.

[18] F. Bonaccorso, T. Hasan, P. H. Tan, C. Sciascia, G. Privitera, G. Di Marco, P. G. Gucciardi, A. C. Ferrari, *J. Phys. Chem. C* **2010**, *114*, 17267.

[19] a)Y. Sasaki, T. Igura, Y.-I. Miyassu, S. Lee, S. Nagadome, H. Takiguchi, G. Sugihara, *Colloid Surface B* **1995**, *5*, 241; b)A. Roda, A. F. Hofmann, K. J. Mysels, *J. Biol. Chem.* **1983**, *258*, 6362.